

DISCONTINUOUS GALERKIN FINITE ELEMENT METHOD FOR
ELECTROMAGNETIC STRUCTURE ANALYSIS: VALIDATION AND
APPLICATIONS

A THESIS SUBMITTED TO
THE GRADUATE SCHOOL OF NATURAL AND APPLIED SCIENCES
OF
MIDDLE EAST TECHNICAL UNIVERSITY

BY

TALHA ÇALIŞ

IN PARTIAL FULFILLMENT OF THE REQUIREMENTS
FOR
THE DEGREE OF MASTER OF SCIENCE
IN
ELECTRICAL AND ELECTRONIC ENGINEERING

September 2024

Approval of the thesis:

**DISCONTINUOUS GALERKIN FINITE ELEMENT METHOD FOR
ELECTROMAGNETIC STRUCTURE ANALYSIS: VALIDATION AND
APPLICATIONS**

submitted by **TALHA ÇALIŞ** in partial fulfillment of the requirements for the degree of **Master of Science in Electrical and Electronic Engineering, Middle East Technical University** by,

Prof. Dr. Naci Emre Altun

Dean, **Graduate School of Natural and Applied Sciences**

Prof. Dr. İlkay Ulusoy

Head of the Department, **Electrical and Electronics Eng.**

Prof. Dr. Mustafa Kuzuoğlu

Supervisor, **Electrical and Electronics Eng., METU**

Examining Committee Members:

Prof. Dr. Gülbin Dural Ünver

Electrical and Electronics Eng, METU

Prof. Dr. Mustafa Kuzuoğlu

Electrical and Electronics Eng, METU

Prof. Dr. Özlem Özgün

Electrical and Electronics Eng, Hacettepe University

Prof. Dr. Asım Egemen Yılmaz

Electrical and Electronics Eng, Ankara University

Assist. Prof. Dr. Ahmet Cemal Durgun

Electrical and Electronics Eng, METU

Date: 05.09.2024

I hereby declare that all information in this document has been obtained and presented in accordance with academic rules and ethical conduct. I also declare that, as required by these rules and conduct, I have fully cited and referenced all material and results that are not original to this work.

Name Last name : Talha Çalış

Signature :

ABSTRACT

DISCONTINUOUS GALERKIN FINITE ELEMENT METHOD FOR ELECTROMAGNETIC STRUCTURE ANALYSIS: VALIDATION AND APPLICATIONS

Çalış, Talha

Master of Science, Electrical and Electronic Engineering

Supervisor: Prof. Dr. Mustafa Kuzuoğlu

September 2024, 54 pages

In the realm of computational electromagnetics, the Discontinuous Galerkin (DG) method stands as a robust and versatile approach for solving complex problems. This thesis focuses on the development and implementation of a three-dimensional Finite Element Method (FEM) solver by utilizing the Discontinuous Galerkin technique. The distinguishing feature of this method lies in its utilization of distinct basis functions across tetrahedral elements, interconnected through flux terms within the governing 2.s. An interior penalty term is introduced to account for the continuity between adjacent basis functions, enabling a seamless representation of discontinuities while preserving computational efficiency.

One of the key advantages of the DG method is its ability to accommodate high-order basis functions. Also, its intrinsic flexibility allows for the seamless integration of distinct domains, enabling the simulation of finite arrays with individual cells.

This study is an attempt to adapt the discontinuous Galerkin method to a three-dimensional finite element method algorithm. The method is verified by means of some practical applications, by using the code developed for this purpose.

Keywords: Computational Electromagnetics, Finite Element Method, Discontinuous Galerkin Method

ÖZ

ELEKTROMANYETİK YAPILARIN ANALİZİ İÇİN SÜREKSİZ GALERKİN SONLU ELEMAN YÖNTEMİ: DOĞRULAMA VE UYGULAMALAR

Çalış, Talha
Yüksek Lisans, Elektrik ve Elektronik Mühendisliği
Tez Yöneticisi: Prof. Dr. Mustafa Kuzuoğlu

Eylül 2018, 54 sayfa

Hesaplamalı elektromanyetik alanında, Süreksiz Galerkin (SG) yöntemi karmaşık problemleri çözmek için sağlam ve çok yönlü bir yaklaşım olarak durmaktadır. Bu tez, Süreksiz Galerkin tekniğini kullanarak geliştirme ve uygulama üzerine odaklanan üç boyutlu Sonlu Elemanlar Metodu (SEM) çözücüsünün geliştirilmesine derinlemesine inmektedir. Bu yöntemin ayırt edici özelliği, tetrahedral elemanlar arasında farklı baz fonksiyonlarının kullanımında, yöneten denklemler içindeki akım terimleri aracılığıyla birbirine bağlanmasıdır. Bitişik baz fonksiyonları arasındaki sürekliliği hesaba katmak için bir içsel ceza terimi tanımlanmış ve böylece kesintisizliklerin sorunsuz bir temsili sağlanırken hesaplama verimliliği korunmuştur.

SG yönteminin ana avantajlarından biri, yüksek dereceli baz fonksiyonlarını barındırma yeteneğidir. Ayrıca, içsel esnekliği farklı alanların sorunsuz

entegrasyonuna izin verir, bu da bireysel hücrelerle sonlu dizilerin simülasyonunu mümkün kılar.

Bu çalışma, Süreksiz Galerkin yöntemini üç boyutlu sonlu elemanlar yöntemi algoritmasına uyarlamaya yönelik bir girişimdir. Yöntem, geliştirilmiş olan yazılım kullanılarak, çeşitli pratik problemler yardımıyla doğrulanmıştır.

Anahtar Kelimeler: Hesaplamalı Elektromanyetik, Sonlu Elemanlar Yöntemi, Süreksiz Galerkin Yöntemi

To my spouse, who has always supported me

ACKNOWLEDGMENTS

The author wishes to express his deepest gratitude to his supervisor Prof. Dr. Mustafa Kuzuođlu for his guidance, advice, criticism, encouragements and insight throughout the research.

The author would also like to thank Dr. Dođanay Dođan for his suggestions and comments. Without his guidance and help, this work would not be possible to complete.

The author is thankful to ASELSAN A.Ş. for giving him the opportunity to pursue this work and for providing the software licenses and the computational resources used during the work.

The author is also grateful to his parents, Fatma alıř, Mehmet alıř, and Mehmet Gven, for their moral support. Additionally, special thanks are extended to his friend Ali Furkan Aslan, who has always listened to him carefully and supported his work with valuable feedback.

Finally, the author is grateful to his daughter, Hmeyra Zehra, for being so adorable and inspiring her father to keep going, and to his beloved spouse, Aslı Beyza alıř, for believing in him and providing unwavering support despite all challenges.

TABLE OF CONTENTS

ABSTRACT.....	v
ÖZ.....	vii
ACKNOWLEDGMENTS.....	x
TABLE OF CONTENTS.....	xi
LIST OF TABLES.....	xiii
LIST OF FIGURES.....	xiv
LIST OF ABBREVIATIONS.....	xv
CHAPTERS	
1 INTRODUCTION.....	1
1.1 Outline of Basic Methods of Computational Electromagnetics and the DG Method.....	1
1.2 Summary of the Thesis.....	5
2 FORMULATION OF THE DISCONTINUOUS GALERKIN BASED FINITE ELEMENT METHOD.....	7
2.1 Wave Equation.....	8
2.2 Basic Theory of the Discontinuous Galerkin Method.....	9
2.2.1 Weak Formulation.....	9
2.2.2 Interior Penalty Term.....	11
2.2.3 Nedgelec Basis Functions.....	15
2.2.4 Handling Flux Terms in DG Formulations.....	21

3	PRACTICAL IMPLEMENTATION AND CASE STUDIES	25
3.1	Eigenvalue Problem of the PEC Cavity.....	27
3.2	Application of DG method to Waveguide Structures	31
3.3	Simulation and Analysis of Microstrip Structures Using DG Method	38
3.4	Antenna Structure	44
4	CONCLUSION	49
5	REFERENCES	53

LIST OF TABLES

TABLES

Table 1: Local node edge labeling	17
Table 2: Local node face labeling	17
Table 3: Analytically calculated and simulated values of the cutoff frequency	30
Table 4: Solution time and memory usage of Eigenmode solver	31
Table 5: Solution time and memory usage of Waveguide solver	37
Table 6: Solution time and memory usage of Microstrip solver	44
Table 7: Solution time and memory usage of antenna solver	46

LIST OF FIGURES

FIGURES

Figure 1: Basis functions are compatible with the adjacent elements' basis in FEM3	
Figure 2: DG method allows that basis functions are disconnected from each other4	
Figure 3: Node and edge labeling in a tetrahedral element.	16
Figure 4: Mesh structure of the cavity	28
Figure 5: Cut-off modes of the cavity	29
Figure 6: a) DG-FEM solution of the first eigenmode of dielectric cavity. b) HFSS solution of the same structure	30
Figure 7: Waveguide structures and port surfaces	32
Figure 8: Analytically calculated TE ₁₀ mode on the port surface	34
Figure 9: a) DG-FEM solution of complex magnitude of waveguide E field. b) HFSS solution of the same structure	36
Figure 10: The comparison of S ₁₁ parameter of the waveguide structure with results from different solvers.....	37
Figure 11: Mesh structure and port surfaces of the microstrip line.....	39
Figure 12: Electric field distribution on the port surface of the microstrip line	39
Figure 13: Electric field distribution along the microstrip line	40
Figure 14: HFSS solution of the electric field distribution along the microstrip line	41
Figure 15: S ₁₁ -parameters of the microstrip line	42
Figure 16: Comparison of S-parameters from different solvers.....	43
Figure 17: Mesh structure of the antenna	45
Figure 18: S ₁₁ parameter graph for the antenna structure	46

LIST OF ABBREVIATIONS

ABBREVIATIONS

FDTD : Finite Difference Time Domain

MoM : Method of Moments

FEM : Finite Element Method

DG : Discontinuous Galerkin

PEC : perfect electric conductor

PMC : perfect magnetic conductor

PDE : partial differential equations

IP : Interior Penalty

ABC : Absorbing Boundary Condition

LT/QN : Linear tangential / Quadratic Normal

EM : Electromagnetics

HFSS : High Frequency Simulation Software

CHAPTER 1

INTRODUCTION

1.1 Outline of Basic Methods of Computational Electromagnetics and the DG Method

Numerical simulations of electromagnetic fields are widely used in engineering and scientific researches. Since analytical solutions of electromagnetic field problems are feasible for a few simple cases, problems with complex geometries and/or material properties necessitate the use of numerical methods. This introduction will start with a discussion related to the advantages and disadvantages of fundamental numerical computational electromagnetics methods such as the Finite Difference Time Domain (FDTD), Method of Moments (MoM), and Finite Element Method (FEM). Then, the focus of this study, the Discontinuous Galerkin (DG) method, will be introduced along with its integration with the FEM method.

In the FDTD method, which is based on the space-time finite difference discretization of Maxwell's equations at the point (x, y, z, t) , the time increment parameter is designated as Δt , and the computational domain is discretized in terms of Yee cells with dimensions Δx , Δy and Δz along the Cartesian coordinate variables. Consequently, the electric and magnetic fields constituting Maxwell's equations are calculated recursively for the next time step, $t+\Delta t$. Thus, the numerical solution of Maxwell's equations is achieved recursively for a boundary/initial value problem. The FDTD method is preferred in many applications, due to its computational simplicity. The computational domain is discretized as a grid composed of Yee cells in the form of rectangular prisms, and it is quite simple to handle objects with arbitrarily defined constitutive parameters. Another important advantage of the FDTD method is the recursive calculations (without the need to solve matrix

equations) in time domain, obtaining solutions (or simulations) for wide band applications with a single run. The main disadvantage of the FDTD method is the staircasing error introduced for problems involving objects with complex geometries, such as curved boundaries.

Method of Moments (MoM) is a numerical technique for the solution electromagnetic boundary value problems formulated as integral equations with kernels which correspond to the Green's functions of the corresponding problem. It is particularly effective in analyzing structures such as antennas and objects modelled as perfect conductor. In MoM, the unknown quantities are chosen as surface/volume currents or charge distributions, and Maxwell's equations are transformed into integral equation in terms of these unknowns. These integral equations describe the relationship between the fields and the sources (currents or charges) in the problem domain. In many electromagnetic scattering and/or radiation problems, and the integral equation is obtained as a linear operator equation in the form $Lf = u$. Then, by using a basis expansion for the unknown and by using the method of weighted residuals, the MoM matrix equation is obtained. MoM method can provide highly accurate solutions by handling various types of boundary conditions such as open boundaries, perfect electric conductors (PEC), and perfect magnetic conductors (PMC). For electrically small problems, where the size of the objects is comparable to the wavelength of interest, MoM can be computationally efficient. However, the MoM approach end up with a full matrix equation, representing the interactions between all subdomains of the MoM discretization. In problems involving electrically large objects, the method can become computationally expensive. The full matrix can lead to substantial memory usage and increased computation time. In addition to this, different types of boundary value problems require different Green's function solutions, which describe the system's response to a point source. This aspect adds complexity to the implementation of MoM, as each problem may necessitate the computation of the Green's function,

which may be difficult to obtain. Additionally, incorporating material properties accurately is another challenging task in MoM method.

The Finite Element Method is another widely used numerical technique for solving electromagnetic field problems. FEM works by discretizing the problem domain into smaller subdomains, called finite elements, which can be of various shapes such as triangles or quadrilaterals in 2D, and tetrahedral or hexahedra in 3D. Within each element, the electromagnetic fields are approximated using basis functions, typically polynomials [3]. These basis functions must be compatible with the basis functions of the adjacent elements, as can be seen in Figure 1 for a 1D case. FEM is particularly powerful in handling complex geometries and material inhomogeneities. The method is used to reduce the original boundary value problem defined by a partial differential equation (PDE) into a system of algebraic equations by using the weak form of the PDE over each finite element and applying appropriate boundary conditions. These algebraic equations are then assembled into a global system, which can be solved numerically to find the field distribution across the entire problem domain [5]-[6].

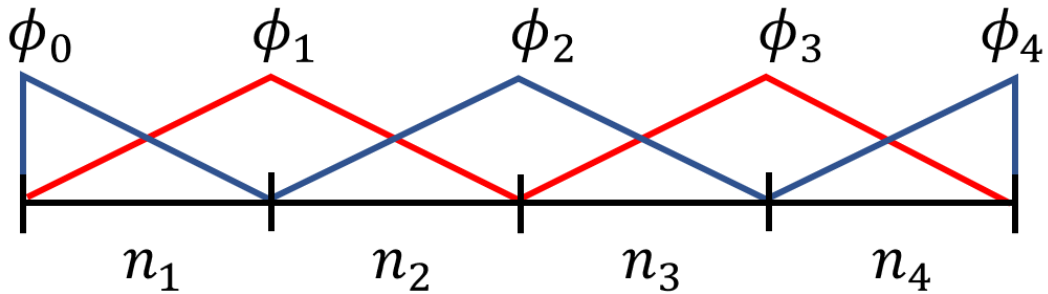


Figure 1: Basis functions are compatible with the adjacent elements' basis in FEM

One of the main advantages of FEM is its flexibility in modeling complex geometries and accurately incorporating material properties. FEM can handle a wide variety of boundary conditions, making it suitable for many different types of electromagnetic problems. Additionally, the method can achieve high accuracy by refining the mesh, i.e., using smaller elements in regions where the field varies

rapidly. However, FEM also has some disadvantages. The method requires a detailed and often computationally intensive meshing process, especially for problems with intricate geometries. As the mesh becomes finer to improve accuracy, the computational resources, including memory and processing power, increase significantly. This can make FEM less efficient for very large or highly complex problems [9].

In this study, the focus is on the Discontinuous Galerkin (DG) method, which combines aspects of FEM with additional flexibility in handling discontinuities in the solution. In the coming paragraphs, the DG method will be introduced and its integration with the FEM method will be discussed, highlighting the advantages it brings to the numerical solution of electromagnetic problems.

The Discontinuous Galerkin method is a numerical approach that combines the benefits of both finite element and finite difference methods [7]-[8]. It is particularly effective in handling problems with discontinuities, such as material interfaces or wave propagation across different media. In the DG method, the problem domain is divided into smaller subdomains, similar to FEM, but instead of enforcing continuity between neighboring elements, DG allows for discontinuities at element interfaces as shown in Figure 2. This flexibility makes DG well-suited for problems involving complex geometries, sharp material transitions, and abruptly varying field distributions [4].

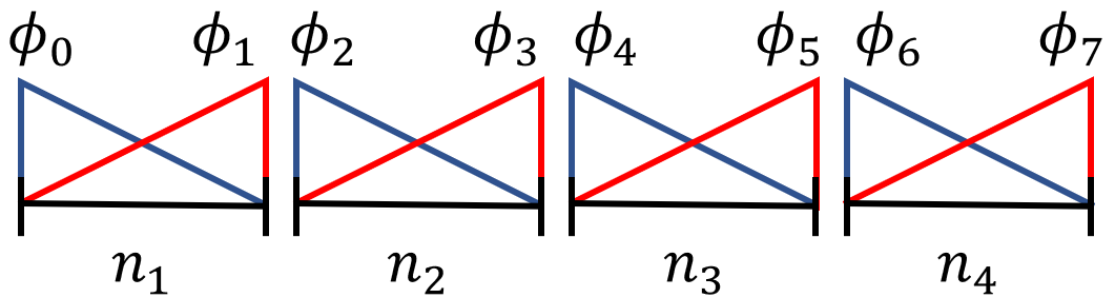


Figure 2: DG method allows that basis functions are disconnected from each other

DG method employs piecewise polynomial approximations within each element, allowing for high-order accuracy in regions of smooth variation while still maintaining stability in the presence of discontinuities. Additionally, DG naturally incorporates local refinement techniques, enabling efficient adaptation of the mesh to capture features of interest with high resolution [10].

One of the key advantages of DG is its ability to accurately capture wave propagation phenomena, including diffraction, dispersion, and reflection, across discontinuities. This makes DG particularly valuable for problems involving guided waves, scattering, and material interfaces. However, DG can also pose challenges, such as increased computational cost compared to traditional FEM methods, especially for problems with highly refined meshes or high-order approximations. Additionally, the implementation of DG requires careful consideration of numerical stability and conservation properties to ensure accurate and reliable results.

In this study, the integration of DG with the Finite Element Method (FEM) will be explored, leveraging the strengths of both methods to overcome the limitations of individual approaches and provide robust and accurate solutions for electromagnetic field problems.

1.2 Summary of the Thesis

The starting point of this study is Maxwell's equations, from which the vector wave equation is derived. In order to convert the vector wave equation into a suitable form for the Discontinuous Galerkin method, the weak form of the wave equation is obtained. Next, domain tessellation and tetrahedral element definitions are provided. It is shown that the stiffness, mass, and flux terms are present in the derived equations as required by the Discontinuous Galerkin method. It is noted that the equations defined on the surface of a tetrahedron would be discontinuous as compared to the equations on the surface of a neighboring tetrahedron. Therefore, unlike the general FEM formulation, the surface integrals in the equations do not cancel out. An interior

penalty term is introduced to handle this discontinuity. The weak formulation is obtained by taking into account the interior penalty definition. Thus, the main equation for numerical implementation is obtained.

Subsequently, as required by the FEM formulation, a set of basis functions is introduced, namely the Nedelec basis. A total of 20 curl-conforming basis functions are constructed for each tetrahedron, and the stiffness and mass matrices are obtained by using these basis functions. Additional terms are derived for the flux contributions, leading to the final numerical formulation.

Next, for practical applications, the Gauss quadrature method is introduced as an integration method followed by a discussion of the algorithm steps. As the first practical application, the PEC cavity problem is introduced, and the PEC boundary condition implementation is provided. The resonance frequency modes in the cavity and the corresponding electric field distributions are calculated by using the method. These calculated modes are compared with analytical results, demonstrating the accuracy of the method. Solution times are compared with those of commercial programs. Subsequently, ports are added to the same geometric model converting it to a waveguide problem, and a solution is obtained for the corresponding waveguide structure. Absorbing Boundary Conditions (ABC) are used to define the ports, and implementation of the ABC formulation is discussed. Port modes are analytically provided to the code as inputs. The electric field distribution is obtained for the waveguide structure and the obtained reflection coefficients are compared with those obtained by commercial programs. Next, a solution is obtained for a microstrip line on a dielectric substrate. Finally, an antenna structure on FR4 material is analyzed. The results and solution times of the microstrip line and the antenna structure are compared with those obtained by commercial codes.

CHAPTER 2

FORMULATION OF THE DISCONTINUOUS GALERKIN BASED FINITE ELEMENT METHOD

Maxwell's equations constitute a set of equations that form the mathematical model for all types of electromagnetic phenomena [1],[2]. They describe the interactions between electric and magnetic fields, known as the electromagnetic field, and material objects. If the problem domain is defined as $\Omega \subseteq \mathbb{R}^3$, then Maxwell's equations are as follows:

$$\nabla \times \vec{E} = -\frac{\partial \vec{B}}{\partial t} \quad \text{in } \Omega \quad (2.1)$$

$$\nabla \times \vec{H} = \frac{\partial \vec{D}}{\partial t} + \vec{J} \quad \text{in } \Omega \quad (2.2)$$

$$\nabla \cdot \vec{D} = \rho \quad \text{in } \Omega \quad (2.3)$$

$$\nabla \cdot \vec{B} = 0 \quad \text{in } \Omega \quad (2.4)$$

\vec{E} (V/m) describes the electric field intensity and \vec{H} (A/m) describes the magnetic field intensity. \vec{D} (C/m) is the electric flux density and \vec{B} (Wb/m²) is the magnetic flux density. \vec{J} (A/m²) describes the electric current density and ρ (C/m³) is the volume charge density.

The fields \vec{E} and \vec{D} and the fields \vec{H} and \vec{B} are related through constitutive relations, which, for a simple medium reduce to

$$\vec{D} = \epsilon \vec{E} \quad (2.5)$$

$$\vec{B} = \mu \vec{H} \quad (2.6)$$

2.1 Wave Equation

The wave equation for the electric field \vec{E} can be obtained from Maxwell's equations, starting with Faraday's law which is given in ((2.1). Taking the curl of this equation, we have:

$$\nabla \times \mu^{-1}(\nabla \times \vec{E}) = -\nabla \times \left(\frac{\partial \vec{H}}{\partial t} \right) \quad (2.7)$$

By substituting (2.2) (Ampere-Maxwell's law), we get:

$$\nabla \times \mu^{-1}(\nabla \times \vec{E}) = -\frac{\partial}{\partial t} \left(\vec{J} + \epsilon \frac{\partial \vec{E}}{\partial t} \right) \quad (2.8)$$

This simplifies to:

$$\nabla \times \mu^{-1}(\nabla \times \vec{E}) = -\epsilon \frac{\partial^2 \vec{E}}{\partial t^2} - \frac{\partial \vec{J}}{\partial t} \quad (2.9)$$

When dealing with time-harmonic fields, the electric and magnetic fields can be expressed in phasor form. In this context, the fields are assumed to vary sinusoidally with time at a single angular frequency ω . Thus, the time-dependent electric and magnetic fields can be represented as:

$$\vec{E}(r, t) = \text{Real}\{\vec{E}(r)e^{j\omega t}\} \quad (2.10)$$

$$\vec{H}(r, t) = \text{Real}\{\vec{H}(r)e^{j\omega t}\} \quad (2.11)$$

Here, $\vec{E}(r)$ and $\vec{H}(r)$ are the complex phasors of the electric and magnetic fields, respectively, ω is the angular frequency, and j is the imaginary unit. The real part is taken to obtain the time-domain fields from their phasor representations. From this stage onward, \vec{E} and \vec{H} will be expressed in phasor form. The equation that expresses the relationship between the electric and magnetic fields in phasor form is as follows:

$$\vec{E}(r) = -\frac{j}{\epsilon\omega} \nabla \times \vec{H}(r) \quad (2.12)$$

Since the electric field is of primary interest in many applications, it is chosen as the unknown field variable throughout this thesis. Equation ((2.9) in phasor form is as follows:

$$\nabla \times \mu^{-1}(\nabla \times \vec{E}) - \omega^2 \epsilon \vec{E} = j\omega \vec{J} \quad (2.13)$$

2.2 Basic Theory of the Discontinuous Galerkin Method

2.2.1 Weak Formulation

As a first step, some notation definitions will be given in this section. As defined before, problem domain is a subset of the three-dimensional space, denoted as $\Omega \subseteq \mathbb{R}^3$, and the boundary of the domain is $\partial\Omega$. Next, the domain is discretized in terms of a mesh (tessellation set) composed of tetrahedra with 4 vertices and 4 triangular faces. Tessellation set is represented by \mathcal{T}_h , and κ_n shows the n'th tetrahedron such that $\kappa_n \in \mathcal{T}_h$. The boundary of this tetrahedron is shown with $\partial\kappa$. Also $\sum_n^{N_t} \kappa_n = \mathcal{T}_h$ and N_t refers the number of tetrahedra.

In contrast to Denissen's work [11], which formulates the DG-FEM method based on the H field, this thesis develops the DG-FEM approach using the E field. Equation ((2.13) can be partitioned into two distinct equations:

$$\nabla \times \mu^{-1} \vec{q} - \omega^2 \epsilon \vec{E} = j\omega \vec{J} \quad (in \Omega) \quad (2.14)$$

$$\vec{q} = \nabla \times \vec{E} \quad (in \Omega) \quad (2.15)$$

Defining the arbitrary test function pair as ϕ, π , these equations can be dot multiplied by the corresponding test functions and the result is integrated over the entire domain. The resulting equation system is:

$$\int_{\Omega} (\nabla \times \mu^{-1} \vec{q}) \cdot \phi \, dV - \omega^2 \epsilon \int_{\Omega} \vec{E} \cdot \phi \, dV = j\omega \int_{\Omega} \vec{J} \cdot \phi \, dV \quad (2.16)$$

$$\int_{\Omega} \vec{q} \cdot \pi \, dV = \int_{\Omega} (\nabla \times \vec{E}) \cdot \pi \, dV \quad (2.17)$$

This equation can be simplified by using the vector identities given below:

$$\begin{aligned} \nabla \cdot (A \times B) &= B \cdot (\nabla \times A) - A \cdot (\nabla \times B) \\ (\nabla \times A) \cdot B &= \nabla \cdot (A \times B) + (\nabla \times B) \cdot A \\ A \cdot (B \times C) &= B \cdot (C \times A) \end{aligned} \quad (2.18)$$

Applying the second vector identity to the first term in Equation ((2.16) and applying the Gauss theorem to the first term in the right hand side, we obtain

$$\begin{aligned} \int_{\Omega} (\nabla \times \mu^{-1} \vec{q}) \cdot \phi \, dV &= \mu^{-1} \int_{\Omega} (\nabla \times \phi) \cdot \vec{q} \, dV + \int_{\Omega} \nabla \cdot (\mu^{-1} \vec{q} \times \phi) \, dV \\ &= \mu^{-1} \int_{\Omega} (\nabla \times \phi) \cdot \vec{q} \, dV + \sum_{\kappa \in \mathcal{J}_h} \int_{\partial \kappa} n \cdot ((\mu^{-1} \vec{q})^* \times \phi) \, dA \\ &= \mu^{-1} \int_{\Omega} (\nabla \times \phi) \cdot \vec{q} \, dV + \sum_{\kappa \in \mathcal{J}_h} \int_{\partial \kappa} \phi \cdot (n \times (\mu^{-1} \vec{q})^*) \, dA \end{aligned}$$

In the equations above, the * symbol is used to indicate that the respective entity is at the boundary surface. Since the DG method allows for discontinuities at these surfaces, it is necessary to define these expressions. Similarly, applying the second vector identity to the first term in the Equation ((2.17) and applying the Gauss theorem to the first term in the right hand side:

$$\begin{aligned} \int_{\Omega} (\nabla \times \vec{E}) \cdot \pi \, dV &= \int_{\Omega} \nabla \cdot (\vec{E} \times \pi) \, dV + \int_{\Omega} (\nabla \times \pi) \cdot \vec{E} \, dV \\ &= \int_{\Omega} (\nabla \times \pi) \cdot \vec{E} \, dV + \sum_{\kappa \in \mathcal{J}_h} \int_{\partial \kappa} n \cdot (\vec{E}^* \times \pi) \, dA \\ &= \int_{\Omega} \pi \cdot (\nabla \times \vec{E}) \, dV - \int_{\Omega} \nabla \cdot (\vec{E} \times \pi) \, dV + \sum_{\kappa \in \mathcal{J}_h} \int_{\partial \kappa} n \cdot (\vec{E}^* \times \pi) \, dA \\ &= \int_{\Omega} \pi \cdot (\nabla \times \vec{E}) \, dV + \sum_{\kappa \in \mathcal{J}_h} \int_{\partial \kappa} n \cdot ((\vec{E}^* - \vec{E}) \times \pi) \, dA \end{aligned}$$

$$= \int_{\Omega} \pi \cdot (\nabla \times \vec{E}) dV + \sum_{\kappa \in \mathcal{T}_h} \int_{\partial\kappa} \pi \cdot (n \times (\vec{E}^* - \vec{E})) dA$$

If we substitute these results into equations ((2.16) and ((2.17), we obtain the weak formulations of the equations:

$$\begin{aligned} \int_{\Omega} \mu^{-1} (\nabla \times \phi) \cdot \vec{q} dV - \omega^2 \epsilon \int_{\Omega} \vec{E} \cdot \phi dV + \sum_{\kappa \in \mathcal{T}_h} \int_{\partial\kappa} \phi \cdot (n \times (\mu^{-1} \vec{q})^*) dA \\ = j\omega \int_{\Omega} \vec{J} \cdot \phi dV \end{aligned} \quad (2.19)$$

$$\int_{\Omega} \vec{q} \cdot \pi dV = \int_{\Omega} \pi \cdot (\nabla \times \vec{E}) dV + \sum_{\kappa \in \mathcal{T}_h} \int_{\partial\kappa} \pi \cdot (n \times (\vec{E}^* - \vec{E})) dA \quad (2.20)$$

2.2.2 Interior Penalty Term

Consider two adjacent tetrahedra denoted by κ_L and κ_R (that is, $\kappa_L, \kappa_R \in \mathcal{T}_h$), sharing the same face f . Let \mathbf{u} be a function that is defined inside κ_L and κ_R , with a tangential jump across the face f [13]-[14].

$$[[u]]_T = n_L \times u_R + n_R \times u_L \quad (2.21)$$

$$\{u\} = \frac{u_L + u_R}{2} \quad (2.22)$$

Let us define $F_n^i, F_n^b \in \partial\kappa_n$ where F_n^i defines the interior faces and F_n^b defines the boundary faces. After these definitions, the following formula can be obtained by summing over the surfaces:

$$\begin{aligned} \sum_{\kappa \in \mathcal{T}_h} \int_{\partial\kappa} (n \times u) \cdot v dA = - \int_{F_n^i} \{u\} \cdot [[v]]_T dA + \int_{F_n^i} \{v\} \cdot [[u]]_T dA \\ + \int_{F_n^b} (n \times u) \cdot v dA \end{aligned} \quad (2.23)$$

If we apply this formula to the relevant terms in ((2.19) and ((2.20), we get:

$$\begin{aligned} \sum_{\kappa \in \mathcal{T}_h} \int_{\partial \kappa} \phi \cdot (n \times (\mu^{-1} \vec{q})^*) dA &= - \int_{F_n^i} \{(\mu^{-1} \vec{q})^*\} \cdot \llbracket \phi \rrbracket_T dA \\ &+ \int_{F_n^i} \{\phi\} \cdot \llbracket (\mu^{-1} \vec{q})^* \rrbracket_T dA + \int_{F_n^b} (n \times (\mu^{-1} \vec{q})^*) \cdot \phi dA \end{aligned}$$

and,

$$\begin{aligned} \sum_{\kappa \in \mathcal{T}_h} \int_{\partial \kappa} \pi \cdot (n \times (\vec{E}^* - \vec{E})) dA &= - \int_{F_n^i} \{(\vec{E}^* - \vec{E})\} \cdot \llbracket \pi \rrbracket_T dA \\ &+ \int_{F_n^i} \{\pi\} \cdot \llbracket (\vec{E}^* - \vec{E}) \rrbracket_T dA + \int_{F_n^b} (n \times (\vec{E}^* - \vec{E})) \cdot \pi dA \end{aligned}$$

These equations can be substituted into equations ((2.19) and ((2.20):

$$\begin{aligned} \int_{\Omega} \mu^{-1} (\nabla \times \phi) \cdot \vec{q} dV - \omega^2 \epsilon \int_{\Omega} \vec{E} \cdot \phi dV - \int_{F_n^i} \{(\mu^{-1} \vec{q})^*\} \cdot \llbracket \phi \rrbracket_T dA \\ + \int_{F_n^i} \{\phi\} \cdot \llbracket (\mu^{-1} \vec{q})^* \rrbracket_T dA + \int_{F_n^b} (n \times (\mu^{-1} \vec{q})^*) \cdot \phi dA = j\omega \int_{\Omega} \vec{J} \cdot \phi dV \end{aligned} \quad (2.24)$$

$$\begin{aligned} \int_{\Omega} \pi \cdot (\nabla \times \vec{E}) dV - \int_{F_n^i} \{\vec{E}^* - \vec{E}\} \cdot \llbracket \pi \rrbracket_T dA + \int_{F_n^i} \{\pi\} \cdot \llbracket \vec{E}^* - \vec{E} \rrbracket_T dA \\ + \int_{F_n^b} (n \times (\vec{E}^* - \vec{E})) \cdot \pi dA = \int_{\Omega} \vec{q} \cdot \pi dV \end{aligned} \quad (2.25)$$

For ease of calculation, a lifting operator should be used to eliminate the defined \vec{q} . The lifting operator simplifies later calculations by transforming local discontinuous variables into a more manageable form. This operator is essential for dealing with the discontinuities at element interfaces, making the integration and solution of these variables more straightforward. By applying the lifting operator, the computational process becomes more efficient and streamlined. Accordingly:

$$\int \mathcal{L}(u) \cdot v dV = \int_{F_n^i} u \cdot \llbracket v \rrbracket_T dA \quad (2.26)$$

$$\int \mathcal{R}(u) \cdot v \, dV = \int_{F_n} u \cdot \{v\} \, dA \quad (2.27)$$

By substituting these equations into equation ((2.25), we get:

$$\int \mathcal{L}(\{\vec{E}^* - \vec{E}\}) \cdot \pi \, dV = \int_{F_n^i} \{\vec{E}^* - \vec{E}\} \cdot \llbracket \pi \rrbracket_T \, dA \quad (2.28)$$

$$\int \mathcal{R}(\llbracket \vec{E}^* - \vec{E} \rrbracket_T) \cdot \pi \, dV = \int_{F_n^i} \llbracket \vec{E}^* - \vec{E} \rrbracket_T \cdot \{\pi\} \, dA + \int_{F_n^b} (n \times (\vec{E}^* - \vec{E})) \cdot \pi \, dA \quad (2.29)$$

So, the following expression can be obtained from equation ((2.25):

$$\begin{aligned} \int_{\Omega} \vec{q} \cdot \pi \, dV &= \int_{\Omega} \pi \cdot (\nabla \times \vec{E}) \, dV - \int \mathcal{L}(\{\vec{E}^* - \vec{E}\}) \cdot \pi \, dV \\ &\quad + \int \mathcal{R}(\llbracket \vec{E}^* - \vec{E} \rrbracket_T) \cdot \pi \, dV \end{aligned} \quad (2.30)$$

According to these results:

$$\vec{q} = \nabla \times \vec{E} - \mathcal{L}(\{\vec{E}^* - \vec{E}\}) + \mathcal{R}(\llbracket \vec{E}^* - \vec{E} \rrbracket_T) \quad (2.31)$$

As a result, equation ((2.24) can be rewritten as:

$$\begin{aligned} \int_{\Omega} \mu^{-1} (\nabla \times \phi) \cdot \left(\nabla \times \vec{E} - \mathcal{L}(\{\vec{E}^* - \vec{E}\}) + \mathcal{R}(\llbracket \vec{E}^* - \vec{E} \rrbracket_T) \right) \, dV \\ - \omega^2 \epsilon \int_{\Omega} \vec{E} \cdot \phi \, dV - \int_{F_n^i} \{(\mu^{-1} \vec{q})^*\} \cdot \llbracket \phi \rrbracket_T \, dA \\ + \int_{F_n^i} \{\phi\} \cdot \llbracket (\mu^{-1} \vec{q})^* \rrbracket_T \, dA + \int_{F_n^b} (n \times (\mu^{-1} \vec{q})^*) \cdot \phi \, dA \\ = j\omega \int_{\Omega} \vec{J} \cdot \phi \, dV \end{aligned} \quad (2.32)$$

Removing the lifting operators, we obtain:

$$\begin{aligned}
& \int_{\Omega} \mu^{-1}(\nabla \times \phi) \cdot (\nabla \times \vec{\mathbf{E}}) dV - \omega^2 \epsilon \int_{\Omega} \vec{\mathbf{E}} \cdot \phi dV \\
& - \int_{F_n^i} \{\vec{\mathbf{E}}^* - \vec{\mathbf{E}}\} \cdot \llbracket \mu^{-1}(\nabla \times \phi) \rrbracket_T dA \\
& + \int_{F_n^i} \llbracket \vec{\mathbf{E}}^* - \vec{\mathbf{E}} \rrbracket_T \cdot \{\mu^{-1}(\nabla \times \phi)\} dA - \int_{F_n^i} \{(\mu^{-1}\vec{\mathbf{q}})^*\} \cdot \llbracket \phi \rrbracket_T dA \\
& + \int_{F_n^i} \{\phi\} \cdot \llbracket (\mu^{-1}\vec{\mathbf{q}})^* \rrbracket_T dA + \int_{F_n^b} (n \times (\vec{\mathbf{E}}^* - \vec{\mathbf{E}})) \cdot (\nabla \times \phi) dA \\
& + \int_{F_n^b} (n \times (\mu^{-1}\vec{\mathbf{q}})^*) \cdot \phi dA = j\omega \int_{\Omega} \vec{\mathbf{J}} \cdot \phi dV
\end{aligned} \tag{2.33}$$

Up to this point, the $*$ symbol has been used to denote discontinuities at mesh surfaces. To handle and penalize these discontinuities, it is necessary to define them clearly. Various methods and functions can be used to describe these discontinuities. One such method is the Interior Penalty Discontinuous Galerkin (IP-DG) method. Accordingly, the flux terms can be defined as follows:

$$\vec{\mathbf{E}}^* = \{\vec{\mathbf{E}}\} \tag{2.34}$$

$$(\mu^{-1}\vec{\mathbf{q}})^* = \{\mu^{-1}\nabla \times \vec{\mathbf{E}}\} - \alpha_f \llbracket (\mu^{-1}\vec{\mathbf{E}})^* \rrbracket_T \tag{2.35}$$

The operators $\{\cdot\}$ and $\llbracket \cdot \rrbracket_T$ in this definition are given by ((2.21) and ((2.22). The parameter α_f in the formulation varies depending on the surface area. The α_f parameter serves as a control parameter for the applied penalty in the formulation and should be optimized.

According to this definition, the interior face integrals can be written as follows:

$$\begin{aligned}
& \int_{F_n^i} \{\vec{\mathbf{E}}^* - \vec{\mathbf{E}}\} \cdot \llbracket \mu^{-1}(\nabla \times \phi) \rrbracket_T dA = 0 \\
& \int_{\Omega} \llbracket \vec{\mathbf{E}}^* - \vec{\mathbf{E}} \rrbracket_T \cdot \{\mu^{-1}(\nabla \times \phi)\} dA = - \int_{\Omega} \llbracket \vec{\mathbf{E}} \rrbracket_T \cdot \{\mu^{-1}(\nabla \times \phi)\} dA
\end{aligned}$$

$$\int_{F_n^i} \{(\mu^{-1}\vec{q})^*\} \cdot \llbracket \phi \rrbracket_T dA = \int_{F_n^i} \{\mu^{-1}\nabla \times \vec{E}\} \cdot \llbracket \phi \rrbracket_T dA - \int_{F_n^i} \alpha_f \llbracket \mu^{-1}\vec{E} \rrbracket_T \cdot \llbracket \phi \rrbracket_T dA$$

$$\int_{F_n^i} \{\phi\} \cdot \llbracket (\mu^{-1}\vec{q})^* \rrbracket_T dA = 0$$

The Interior Penalty Discontinuous Galerkin formulation can be given now as follows:

$$D^{IP}(\vec{E}, \phi) = \mathfrak{S}^{IP}(\phi) \quad (2.36)$$

Where $D^{IP}(\vec{E}, \phi)$ and $\mathfrak{S}^{IP}(\phi)$ are expressed as:

$$D^{IP}(\vec{E}, \phi) = \int_{\Omega} \mu^{-1}(\nabla \times \phi) \cdot (\nabla \times \vec{E}) dV - \omega^2 \epsilon \int_{\Omega} \vec{E} \cdot \phi dV$$

$$- \int_{F_n^i} \llbracket \vec{E} \rrbracket_T \cdot \{\mu^{-1}(\nabla \times \phi)\} dA - \int_{F_n^i} \{\mu^{-1}\nabla \times \vec{E}\} \cdot \llbracket \phi \rrbracket_T dA \quad (2.37)$$

$$+ \int_{F_n^i} \alpha_f \llbracket \mu^{-1}\vec{E} \rrbracket_T \cdot \llbracket \phi \rrbracket_T dA$$

$$\mathfrak{S}^{IP}(\phi) = j\omega \int_{\Omega} \vec{J} \cdot \phi dV + \int_{F_n^b} \alpha_f \mu^{-1} \vec{g} \cdot (n \times \phi) dA$$

$$- \int_{F_n^b} \vec{g} \cdot (\nabla \times \phi) dA \quad (2.38)$$

Where $\vec{g} = n \times \vec{E}^*$.

2.2.3 Nedelec Basis Functions

In the context of the Discontinuous Galerkin (DG) method for solving Maxwell's equations, the choice of basis functions is crucial for accurately representing the electromagnetic fields within each element of the mesh. Nédélec basis functions, introduced by Jean-Claude Nédélec in the early 1980s [12], are particularly well-suited for this purpose. These functions are designed to handle vector fields and ensure the correct representation of tangential continuity of the fields across element boundaries, which is essential for electromagnetic problems.

Nédélec basis functions, which belong to the family of edge elements, are vector-valued and associated with the edges of the mesh elements rather than the vertices. This edge association allows them to naturally enforce the tangential continuity of the electric and magnetic fields, a requirement derived from Maxwell's equations. A notable characteristic of Nédélec basis functions is that they are curl-conformal. This means they are specifically constructed to ensure that the curl of the basis functions, which represents rotational field properties, is accurately captured within the numerical method. This property is essential for correctly representing the rotational nature of electromagnetic fields, which is inherent in Maxwell's curl equations.

Nédélec basis functions and the stiffness and mass terms found in Equation ((2.37) will be defined with reference to Savage's paper [15]. Linear-tangent and quadratic-normal (LT/QN) elements will be used. LT/QN basis functions have 12 edge-based and 8 face-based functions. Figure 3 shows the tetrahedral structure and labeling.

and **Hata! Başvuru kaynağı bulunamadı.** show the edge and face labeling according to Figure 3.

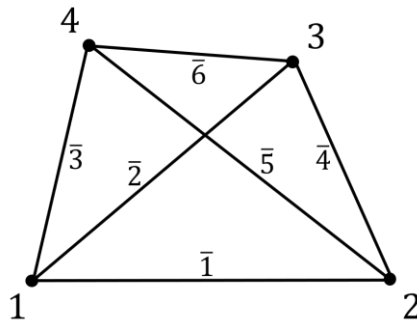


Figure 3: Node and edge labeling in a tetrahedral element.

Table 1: Local node edge labeling

Edge #	Node 1	Node 2
1	1	2
2	1	3
3	1	4
4	2	3
5	2	4
6	3	4

Table 2: Local node face labeling.

Face #	Node 1	Node 2	Node 3
1	1	2	3
2	1	2	4
3	1	3	4
4	2	3	4

Equation ((2.33) has two terms, which are called stiffness and mass terms. The stiffness term arises from the spatial discretization of the PDE and represents the contribution of the gradients or derivatives of the basis functions. It essentially captures how the field variables (such as the electric field \vec{E}) interact with each other

across the spatial domain. Mathematically, the stiffness matrix \mathbf{S} in the context of Maxwell's equations can be expressed as:

$$\mathbf{S}_{ij} = \int_{\Omega} (\nabla \times N_i) \cdot (\nabla \times N_j) d\Omega \quad (2.39)$$

where N_i and N_j are the basis functions, and Ω is the domain of integration.

The mass term represents the inertia or storage of the field variables in the domain. The mass matrix \mathbf{M} can be written as:

$$\mathbf{M}_{ij} = \int_{\Omega} N_i \cdot N_j d\Omega \quad (2.40)$$

For a given tetrahedron, (x_i, y_i, z_i) is the local coordinates for node i . Barycentric coefficients can be computed from the inverse of the matrix containing these coordinates as follow:

$$\begin{bmatrix} b_1 & c_1 & d_1 & a_1 \\ b_2 & c_2 & d_2 & a_2 \\ b_3 & c_3 & d_3 & a_3 \\ b_4 & c_4 & d_4 & a_4 \end{bmatrix} = \begin{bmatrix} x_1 & x_2 & x_3 & x_4 \\ y_1 & y_2 & y_3 & y_4 \\ z_1 & z_2 & z_3 & z_4 \\ 1 & 1 & 1 & 1 \end{bmatrix}^{-1} \quad (2.41)$$

a_i, b_i, c_i, d_i are barycentric coefficients. Barycentric coordinates for an arbitrary node is given as

$$L_i = a_i + b_i x + c_i y + d_i z \quad (2.42)$$

where $i = 1, \dots, 4$. Also the gradient of this coordinate will be used in formulation.

$$\nabla L_i = b_i x + c_i y + d_i z \quad (2.43)$$

Now LT/QN basis functions can be defined as

$$\left. \begin{aligned} N_i^{e1} &= l_i L_{i1} \nabla L_{i2} \\ N_i^{e2} &= l_i L_{i2} \nabla L_{i1} \end{aligned} \right\} \quad i = 1, \dots, 6 \quad (2.44)$$

$$\left. \begin{aligned} N_i^{f1} &= L_{i1} L_{i2} \nabla L_{i3} - L_{i1} L_{i3} \nabla L_{i2} \\ N_i^{f2} &= L_{i1} L_{i2} \nabla L_{i3} - L_{i2} L_{i3} \nabla L_{i1} \end{aligned} \right\} \quad i = 1, \dots, 4 \quad (2.45)$$

where l_i is the length of the edge and e1, e2 denote the first and second type of edge-based basis functions and f1, f2 denote the first and second type of face-based basis functions. Using these basis functions, it is possible to construct the stiffness and mass matrices \mathbf{S} and \mathbf{M} from equations ((2.39) and ((2.40). For example

$$S_{ij}^{e1f1} = \int_V (\nabla \times N_i^{e1}) \cdot (\nabla \times N_j^{f1}) d\Omega$$

All interactions of these 4 types of basis functions construct the stiffness and mass matrices as follows:

$$\mathbf{S} = \begin{bmatrix} S^{e1e1} & S^{e1e2} & S^{e1f1} & S^{e1f2} \\ S^{e2e1} & S^{e2e2} & S^{e2f1} & S^{e2f2} \\ S^{f1e1} & S^{f1e2} & S^{f1f1} & S^{f1f2} \\ S^{f2e1} & S^{f2e2} & S^{f2f1} & S^{f2f2} \end{bmatrix} \quad (2.46)$$

and,

$$\mathbf{M} = \begin{bmatrix} M^{e1e1} & M^{e1e2} & M^{e1f1} & M^{e1f2} \\ M^{e2e1} & M^{e2e2} & M^{e2f1} & M^{e2f2} \\ M^{f1e1} & M^{f1e2} & M^{f1f1} & M^{f1f2} \\ M^{f2e1} & M^{f2e2} & M^{f2f1} & M^{f2f2} \end{bmatrix} \quad (2.47)$$

For calculating these elements, the following operators should be defined:

$$v_{ij} = \nabla L_i \times \nabla L_j \quad (2.48)$$

$$\vartheta_{ij} = \nabla L_i \cdot \nabla L_j \quad (2.49)$$

$$Z_{ij} = \frac{1}{V} \int_V L_i L_j dV \quad (2.50)$$

$$N_{ijk} = \frac{1}{V} \int_V L_i L_j L_k dV \quad (2.51)$$

$$P_{ijkl} = \frac{1}{V} \int_V L_i L_j L_k L_l dV \quad (2.52)$$

V denotes the volume of the tetrahedron. Now it is possible to define all elements of the \mathbf{S} and \mathbf{M} matrices:

$$\begin{aligned}
S_{ij}^{e1e1} &= Vl_i l_j (v_{i1,i2} \cdot v_{j1,j2}) \\
S_{ij}^{e1e2} &= -S_{ij}^{e1e1} \\
S_{ij}^{e2e2} &= S_{ij}^{e1e1} \\
S_{ij}^{e1f1} &= \frac{Vl_i}{4} v_{i1,i2} \cdot (2v_{j2,j3} + v_{j1,j3} - v_{j1,j2}) \\
S_{ij}^{e2f1} &= -E_{ij}^{e1f1} \\
S_{ij}^{f1f1} &= V(4Z_{i1,j1} v_{i2,i3} \cdot v_{j2,j3} \\
&\quad + 2Z_{i1,j2} v_{i2,i3} \cdot v_{j1,j3} \\
&\quad - 2Z_{i1,j3} v_{i2,i3} \cdot v_{j1,j2} \\
&\quad + 2Z_{i2,j1} v_{i1,i3} \cdot v_{j2,j3} \\
&\quad + Z_{i2,j2} v_{i1,i3} \cdot v_{j1,j3} \\
&\quad - Z_{i2,j3} v_{i1,i3} \cdot v_{j1,j2} \\
&\quad - 2Z_{i3,j1} v_{i1,i2} \cdot v_{j2,j3} \\
&\quad - Z_{i3,j2} v_{i1,i2} \cdot v_{j1,j3} \\
&\quad + Z_{i3,j3} v_{i1,i2} \cdot v_{j1,j2}) \\
S_{ij}^{e1f2} &= \frac{Vl_i}{4} v_{i1,i2} \cdot (v_{j2,j3} + 2v_{j1,j3} + v_{j1,j2}) \\
S_{ij}^{e2f2} &= -S_{ij}^{e1f2} \\
S_{ij}^{f1f2} &= V(2Z_{i1,j1} v_{i2,i3} \cdot v_{j2,j3} \\
&\quad + 4Z_{i1,j2} v_{i2,i3} \cdot v_{j1,j3} \\
&\quad + 2Z_{i1,j3} v_{i2,i3} \cdot v_{j1,j2} \\
&\quad + Z_{i2,j1} v_{i1,i3} \cdot v_{j2,j3} \\
&\quad + 2Z_{i2,j2} v_{i1,i3} \cdot v_{j1,j3} \\
&\quad + Z_{i2,j3} v_{i1,i3} \cdot v_{j1,j2} \\
&\quad - Z_{i3,j1} v_{i1,i2} \cdot v_{j2,j3} \\
&\quad - 2Z_{i3,j2} v_{i1,i2} \cdot v_{j1,j3} \\
&\quad - Z_{i3,j3} v_{i1,i2} \cdot v_{j1,j2}) \\
S_{ij}^{f2f2} &= V(Z_{i1,j1} v_{i2,i3} \cdot v_{j2,j3} \\
&\quad + 2Z_{i1,j2} v_{i2,i3} \cdot v_{j1,j3} \\
&\quad + Z_{i1,j3} v_{i2,i3} \cdot v_{j1,j2} \\
&\quad + 2Z_{i2,j1} v_{i1,i3} \cdot v_{j2,j3} \\
&\quad + 4Z_{i2,j2} v_{i1,i3} \cdot v_{j1,j3} \\
&\quad + 2Z_{i2,j3} v_{i1,i3} \cdot v_{j1,j2} \\
&\quad + Z_{i3,j1} v_{i1,i2} \cdot v_{j2,j3} \\
&\quad + 2Z_{i3,j2} v_{i1,i2} \cdot v_{j1,j3} \\
&\quad + Z_{i3,j3} v_{i1,i2} \cdot v_{j1,j2})
\end{aligned} \tag{2.53}$$

$$\begin{aligned}
M_{ij}^{e1e1} &= Vl_i l_j \vartheta_{i2,j2} Z_{i1,j1} \\
M_{ij}^{e1e2} &= Vl_i l_j \vartheta_{i2,j1} Z_{i1,j2} \\
M_{ij}^{e2e2} &= Vl_i l_j \vartheta_{i1,j1} Z_{i2,j2} \\
M_{ij}^{e1f1} &= Vl_i (\vartheta_{i2,j3} N_{i1,j1,j2} - \vartheta_{i2,j2} N_{i1,j1,j3}) \\
M_{ij}^{e2f1} &= Vl_i (\vartheta_{i1,j3} N_{i2,j1,j2} - \vartheta_{i1,j2} N_{i2,j1,j3}) \\
M_{ij}^{f1f1} &= V (\vartheta_{i3,j3} P_{i1,i2,j1,j2} - \vartheta_{i3,j2} P_{i1,i2,j1,j3} - \vartheta_{i2,j3} P_{i1,i3,j1,j2} \\
&\quad + \vartheta_{i2,j2} P_{i1,i3,j1,j3}) \\
M_{ij}^{e1f2} &= Vl_i (\vartheta_{i2,j3} N_{i1,j1,j2} - \vartheta_{i2,j1} N_{i1,j2,j3}) \\
M_{ij}^{e2f2} &= Vl_i (\vartheta_{i1,j3} N_{i2,j1,j2} - \vartheta_{i1,j1} N_{i2,j2,j3}) \\
M_{ij}^{f1f2} &= V (\vartheta_{i3,j3} P_{i1,i2,j1,j2} - \vartheta_{i3,j1} P_{i1,i2,j2,j3} - \vartheta_{i2,j3} P_{i1,i3,j1,j2} \\
&\quad + \vartheta_{i2,j1} P_{i1,i3,j2,j3}) \\
M_{ij}^{f2f2} &= V (\vartheta_{i3,j3} P_{i1,i2,j1,j2} - \vartheta_{i3,j1} P_{i1,i2,j2,j3} - \vartheta_{i1,j3} P_{i2,i3,j1,j2} \\
&\quad + \vartheta_{i1,j1} P_{i2,i3,j2,j3})
\end{aligned} \tag{2.54}$$

Along with the definition of these terms, the first two terms in Equation ((2.37), namely the stiffness and mass terms, are expressed in matrix form. Additionally, Nédélec-type basis functions are introduced. There are 12 edge-based basis functions: 6 for edge type 1 and 6 for edge type 2. For face-based basis functions, there are 8 in total: 4 for face type 1 and 4 for face type 2. In total, 20 basis functions are introduced. The same basis functions will be used for each mesh. Since the stiffness and mass matrices are also 20x20 in size, the block-diagonalized matrices corresponding to the tetrahedron are obtained in the overall matrix.

2.2.4 Handling Flux Terms in DG Formulations

The first two terms in Equation ((2.37), the stiffness and mass terms, are derived and expressed by Equations ((2.46) and ((2.47). However, in Equation ((2.37), the flux terms, which account for the discontinuities at the surfaces, also need to be derived. The derivation of the flux terms will be given in this section. In

the Discontinuous Galerkin (DG) method, flux terms represent the exchange of information and discontinuities at element interfaces. Unlike the standard FEM, where solutions are continuous across elements, the DG method allows for independent solutions within each element. Flux terms, such as numerical flux and interior penalty, facilitate communication between elements and manage numerical instabilities at interfaces. In FEM, the continuity of functions at shared nodes eliminates the need for flux terms. The derivation of flux terms involves surface integrals at element boundaries, ensuring the stability and accuracy of the DG method by penalizing discontinuities and enabling consistent transitions between elements [11].

The first two flux terms from Equation ((2.37) are given as:

$$\int_{F_n^i} \llbracket \vec{E} \rrbracket_T \cdot \{\mu^{-1}(\nabla \times \phi)\} dA + \int_{F_n^i} \{\mu^{-1} \nabla \times \vec{E}\} \cdot \llbracket \phi \rrbracket_T dA \quad (2.55)$$

So far, ϕ has been considered as any basis function. However, after the introduction of Nédélec-type basis functions, ϕ can now be specified as LT/QN Nédélec-type basis functions. Considering only a single tetrahedron, the boundary conditions F_n^i are the sum of the four faces of the tetrahedron. Accordingly, the integrals can be considered as the sum of the integrals over the four different faces of a tetrahedron. By using Equation ((2.21) and ((2.22), it can be written that:

$$\begin{aligned} & \sum_{\substack{\partial\kappa \\ \kappa=\kappa_L}} \int_{\partial\kappa} \left((n_L \times \vec{E}^L) + (n_R \times \vec{E}^R) \right) \cdot \frac{1}{2} \left((\mu^{-1})^L (\nabla \times \phi_{i,\kappa_L}) \right) dA \\ & + \sum_{\substack{\partial\kappa \\ \kappa=\kappa_R}} \int_{\partial\kappa} \left((n_L \times \vec{E}^L) + (n_R \times \vec{E}^R) \right) \cdot \frac{1}{2} \left((\mu^{-1})^R (\nabla \times \phi_{i,\kappa_R}) \right) dA \\ & + \sum_{\substack{\partial\kappa \\ \kappa=\kappa_L}} \int_{\partial\kappa} \frac{1}{2} \left((\mu^{-1})^L (\nabla \times \vec{E}^L) + (\mu^{-1})^R (\nabla \times \vec{E}^R) \right) \cdot (n_L \times \phi_{i,\kappa_L}) dA \\ & + \sum_{\substack{\partial\kappa \\ \kappa=\kappa_R}} \int_{\partial\kappa} \frac{1}{2} \left((\mu^{-1})^L (\nabla \times \vec{E}^L) + (\mu^{-1})^R (\nabla \times \vec{E}^R) \right) \cdot (n_R \times \phi_{i,\kappa_R}) dA \end{aligned} \quad (2.56)$$

Substituting the basis function into \vec{E}^L and \vec{E}^R ,

$$\begin{aligned}
&= \sum_{\kappa=\kappa_L}^{\partial\kappa} \sum_{j=1}^{n_p} u_{j,\kappa_L} \int_{\partial\kappa} \frac{1}{2} \left((n_L \times \phi_{j,\kappa_L}) \right) \cdot \left((\mu^{-1})^L (\nabla \times \phi_{i,\kappa_L}) \right) dA \\
&+ \sum_{\kappa=\kappa_L}^{\partial\kappa} \sum_{j=1}^{n_p} u_{j,\kappa_R} \int_{\partial\kappa} \frac{1}{2} \left((n_R \times \phi_{j,\kappa_R}) \right) \cdot \left((\mu^{-1})^L (\nabla \times \phi_{i,\kappa_L}) \right) dA \\
&+ \sum_{\kappa=\kappa_R}^{\partial\kappa} \sum_{j=1}^{n_p} u_{j,\kappa_L} \int_{\partial\kappa} \frac{1}{2} \left((n_L \times \phi_{j,\kappa_L}) \right) \cdot \left((\mu^{-1})^R (\nabla \times \phi_{i,\kappa_R}) \right) dA \\
&+ \sum_{\kappa=\kappa_R}^{\partial\kappa} \sum_{j=1}^{n_p} u_{j,\kappa_R} \int_{\partial\kappa} \frac{1}{2} \left((n_R \times \phi_{j,\kappa_R}) \right) \cdot \left((\mu^{-1})^R (\nabla \times \phi_{i,\kappa_R}) \right) dA \\
&+ \sum_{\kappa=\kappa_L}^{\partial\kappa} \sum_{j=1}^{n_p} u_{j,\kappa_L} \int_{\partial\kappa} \frac{1}{2} (\mu^{-1})^L (\nabla \times \phi_{i,\kappa_L}) \cdot \left((n_L \times \phi_{i,\kappa_L}) \right) dA \\
&+ \sum_{\kappa=\kappa_L}^{\partial\kappa} \sum_{j=1}^{n_p} u_{j,\kappa_R} \int_{\partial\kappa} \frac{1}{2} (\mu^{-1})^R (\nabla \times \phi_{i,\kappa_R}) \cdot \left((n_L \times \phi_{i,\kappa_L}) \right) dA \\
&+ \sum_{\kappa=\kappa_R}^{\partial\kappa} \sum_{j=1}^{n_p} u_{j,\kappa_L} \int_{\partial\kappa} \frac{1}{2} (\mu^{-1})^L (\nabla \times \phi_{i,\kappa_L}) \cdot \left((n_R \times \phi_{i,\kappa_R}) \right) dA \\
&+ \sum_{\kappa=\kappa_R}^{\partial\kappa} \sum_{j=1}^{n_p} u_{j,\kappa_R} \int_{\partial\kappa} \frac{1}{2} (\mu^{-1})^R (\nabla \times \phi_{i,\kappa_R}) \cdot \left((n_R \times \phi_{i,\kappa_R}) \right) dA
\end{aligned} \tag{2.57}$$

The same operations must also be applied to the last term in Equation ((2.37)) to ensure consistency. This involves considering the contributions from all four faces of the tetrahedron and summing the integrals over these faces.

$$\int_{F_n^i} \alpha_f \llbracket \mu^{-1} \vec{E} \rrbracket_T \cdot \llbracket \phi \rrbracket_T dA \tag{2.58}$$

With the use of Equations ((2.21) and ((2.22), the expression can be rewritten in the following way:

$$\begin{aligned}
& \sum_{\substack{\partial\kappa \\ \kappa=\kappa_L}} \int_{\partial\kappa} \alpha_f \left((\mu^{-1})^L (n_L \times \vec{E}^L) + (\mu^{-1})^R (n_R \times \vec{E}^R) \right) \cdot (n_L \times \phi_{i,\kappa_L}) dA \\
& + \sum_{\substack{\partial\kappa \\ \kappa=\kappa_L}} \int_{\partial\kappa} \alpha_f \left((\mu^{-1})^L (n_L \times \vec{E}^L) + (\mu^{-1})^R (n_R \times \vec{E}^R) \right) \cdot (n_R \times \phi_{i,\kappa_R}) dA
\end{aligned} \tag{2.59}$$

By substituting the basis function into E^L and E^R , we ensure that the expressions are correctly formulated within the context of the given framework.

$$\begin{aligned}
& = \sum_{\substack{\partial\kappa \\ \kappa=\kappa_L}} \sum_{j=1}^{n_p} u_{j,\kappa_L} \int_{\partial\kappa} \alpha_f (\mu^{-1})^L (n_L \times \phi_{j,\kappa_L}) \cdot (n_L \times \phi_{i,\kappa_L}) dA \\
& + \sum_{\substack{\partial\kappa \\ \kappa=\kappa_L}} \sum_{j=1}^{n_p} u_{j,\kappa_R} \int_{\partial\kappa} \alpha_f (\mu^{-1})^R (n_R \times \phi_{j,\kappa_R}) \cdot (n_L \times \phi_{i,\kappa_L}) dA \\
& + \sum_{\substack{\partial\kappa \\ \kappa=\kappa_R}} \sum_{j=1}^{n_p} u_{j,\kappa_L} \int_{\partial\kappa} \alpha_f (\mu^{-1})^L (n_L \times \phi_{j,\kappa_L}) \cdot (n_R \times \phi_{i,\kappa_R}) dA \\
& + \sum_{\substack{\partial\kappa \\ \kappa=\kappa_R}} \sum_{j=1}^{n_p} u_{j,\kappa_R} \int_{\partial\kappa} \alpha_f (\mu^{-1})^R (n_R \times \phi_{j,\kappa_R}) \cdot (n_R \times \phi_{i,\kappa_R}) dA
\end{aligned} \tag{2.60}$$

κ_L and κ_R are adjacent elements and their common faces is denoted as $\partial\kappa$. Previously, while constructing the stiffness and mass matrices, 20x20 block matrices were created for all tetrahedra. The total number of these matrices is N_t , and the global stiffness and mass matrices are the block diagonalized forms obtained from the assembly of these matrices. It is clear that these terms cannot establish the connection between tetrahedra, as all terms are related to the basis functions of the corresponding tetrahedron. However, since flux terms are calculated by using the surface elements of the neighboring tetrahedra, these terms ensure the correlation between meshes. In this way, a global FEM matrix for the DG method is obtained.

CHAPTER 3

PRACTICAL IMPLEMENTATION AND CASE STUDIES

This chapter focuses on the practical implementation and case studies of an Electromagnetic (EM) solver utilizing the Discontinuous Galerkin (DG) method within the Finite Element Method (FEM) framework. The main goal is to construct a bridge connecting the theoretical foundations discussed in the previous chapter with real-world applications, demonstrating how the DG-FEM approach can effectively solve complex EM problems. Key topics include the numerical discretization of Maxwell's equations using DG methods, integration techniques like Gauss quadrature for precise calculations, and tailored boundary conditions essential for accurate EM simulations.

The Gauss quadrature method is a widely used numerical integration technique for computing definite integrals with high accuracy, particularly suited for complex functions or integrands represented by high-degree polynomials. This method employs a set of specific weights and points to approximate the integral of a given function. These points (Gauss points) and corresponding weights allow for precise estimation of the integral at known locations. The Gauss quadrature method is used to approximate the definite integral of a specific function using a weighted sum formula. Typically, the approximate value of the integral is calculated as:

$$\int_a^b f(x) dx \approx \sum_{i=1}^n w_i \cdot f(x_i) \quad (3.1)$$

Here,

- w_i : Weights corresponding to the Gauss points.
- x_i : Gauss points.

The Gauss quadrature method computes the approximate value of the integral by selecting Gauss points and their corresponding weights. These points and weights are derived using specific mathematical formulations tailored to the function being integrated. This method provides results close to the exact value of the integral, especially for integrals represented by high-degree polynomials or complex functions. In chapter 2, it has been discussed that especially for calculating the flux terms, some definite integrals should be computed. These integrals are numerically evaluated by using the Gauss quadrature method.

In this chapter, some case studies will be given that demonstrate the versatility and performance of the EM solver across different applications. These case studies include solving the cavity problem, analyzing waveguide structures, simulating microstrip lines, and designing antennas. Each study demonstrates the solver's ability to effectively handle complex geometries, manage discontinuities inherent in EM simulations, and deliver accurate results for practical engineering scenarios.

As a specific example, the framework for the algorithm is given below for the cavity problem. Solutions for the other problems are built upon this main framework with some modifications.

- Define the frequency (f), speed of light (c), wavelength (λ), and other constants.
- Define Gauss quadrature coefficients and points.
- Load the mesh. Specify the constitutive parameters. Determine the index of each tetrahedron and the indices of all four faces.
- Determine the neighbors of each tetrahedron and create a table of neighbor element indices and face indices for each mesh surface.
- Define the master tetrahedron.
- Calculate the edge lengths of each edge of each element.
- For each face of each element:
 - Compute Gauss points.

- Calculate basis functions at Gauss points using the equations provided in ((2.44) and ((2.45). Two different bases should be calculated at the same points for κ_L and κ_R .
- Calculate flux terms given by equations ((2.56) and ((2.57) using the basis functions. The defined integrals in the terms are computed using the Gauss quadrature formula given by equation (3.1).
- Insert the obtained matrices (of size $20*N_t$, $20*N_t$) in the corresponding positions of the global sparse matrix.
- For each element
 - Construct the 20×20 stiffness matrix using the formulas given by ((2.53).
 - Create the 20×20 mass matrix using the formulas given by ((2.54).
 - Insert the obtained matrices in block diagonal form according to their element order and place them into the global FEM matrix.
- Obtain matrices for the generalized eigenvalue problem by using equation ((2.37).
- Solve the generalized eigenvalue problem.
- Filter out spurious solutions.
- Plot the results.

3.1 Eigenvalue Problem of the PEC Cavity

The eigenvalue problem of a PEC cavity involves finding the resonant frequencies (eigenvalues) and the corresponding field distributions (eigenmodes) of electromagnetic waves within a cavity. A cavity is a region in space bounded by a medium that confines electromagnetic waves. The eigenvalue problem is central to understanding how these waves resonate within the cavity.

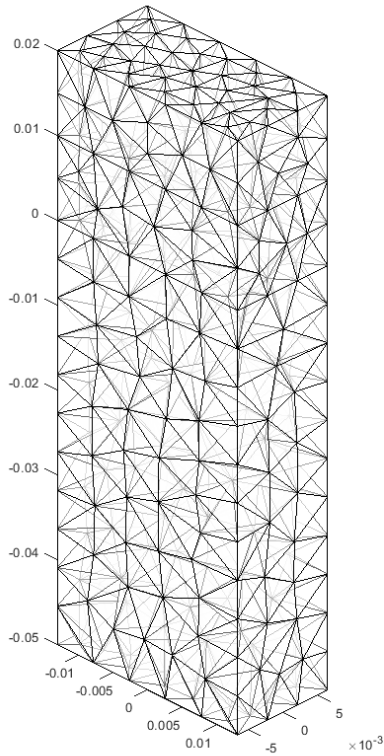


Figure 4: Mesh structure of the cavity

In numerical methods, the eigenvalue problem often serves as the initial test to verify the functionality of a solver due to its relatively straightforward nature. Solving for the eigenvalues and eigenmodes provides a clear indication of whether the solver is correctly implemented and capable of handling more complex problems. This preliminary check is essential in the development and validation of numerical solvers, ensuring that they can accurately model the physical phenomena under study. In this study, the cavity model shown in Figure 4 was used for the solution. The model consists of 1902 tetrahedral elements. Cavity dimensions are 70x26x13mm and the cavity is filled with vacuum.

For this cavity model, it is necessary to define appropriate boundary conditions to accurately solve the eigenvalue problem. One commonly used boundary condition is the PEC boundary condition. PEC boundaries enforce that the

tangential component of the electric field is zero on the surface, effectively confining the electromagnetic waves within the cavity:

$$n \times \vec{E} = 0 \quad (3.2)$$

This condition is critical for the accurate determination of the resonant frequencies and field distributions, as it reflects the physical reality of many practical applications where metallic boundaries are present. Thus, implementing PEC boundary conditions is mandatory for a realistic and precise solution to the eigenvalue problem in a PEC cavity.

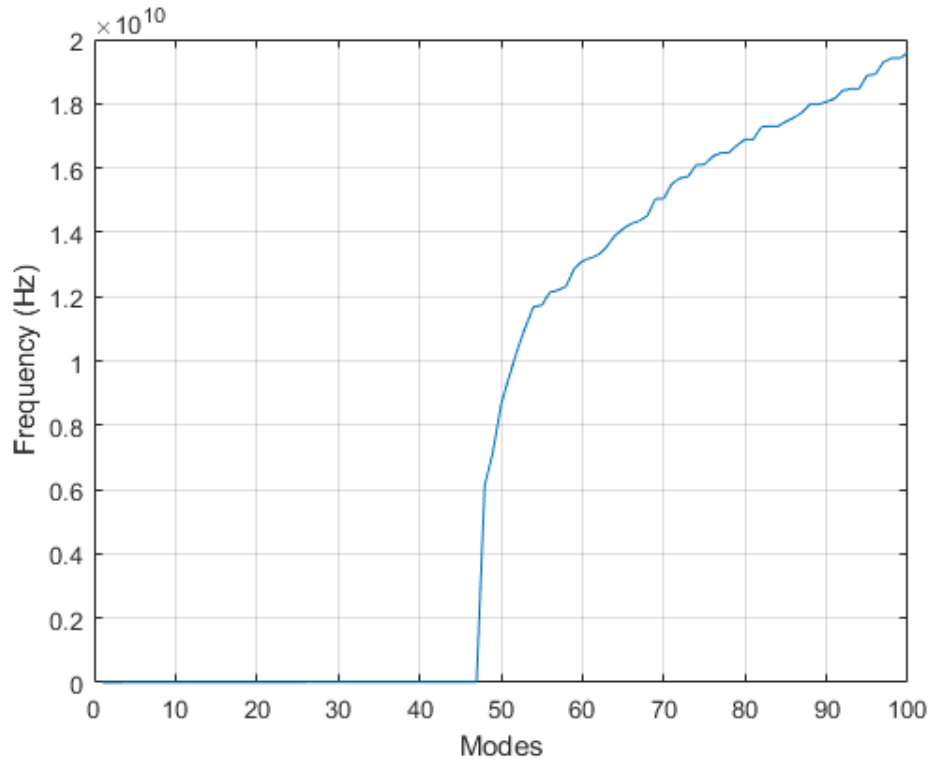


Figure 5: Cut-off modes of the cavity

The results of the eigenvalue problem solution are depicted in Figure 5, which shows the cut-off modes of the cavity. Table 3 lists the analytically calculated and simulated values of the cutoff frequencies for the first three modes.

Table 3: Analytically calculated and simulated values of the cutoff frequency

Modes	Calculated Cutoff Frequency (GHz)	Exact Cutoff Frequency (GHz)
TE110	6.141	6.1543
TE210	7.159	7.1869
TE310	8.624	8.6377

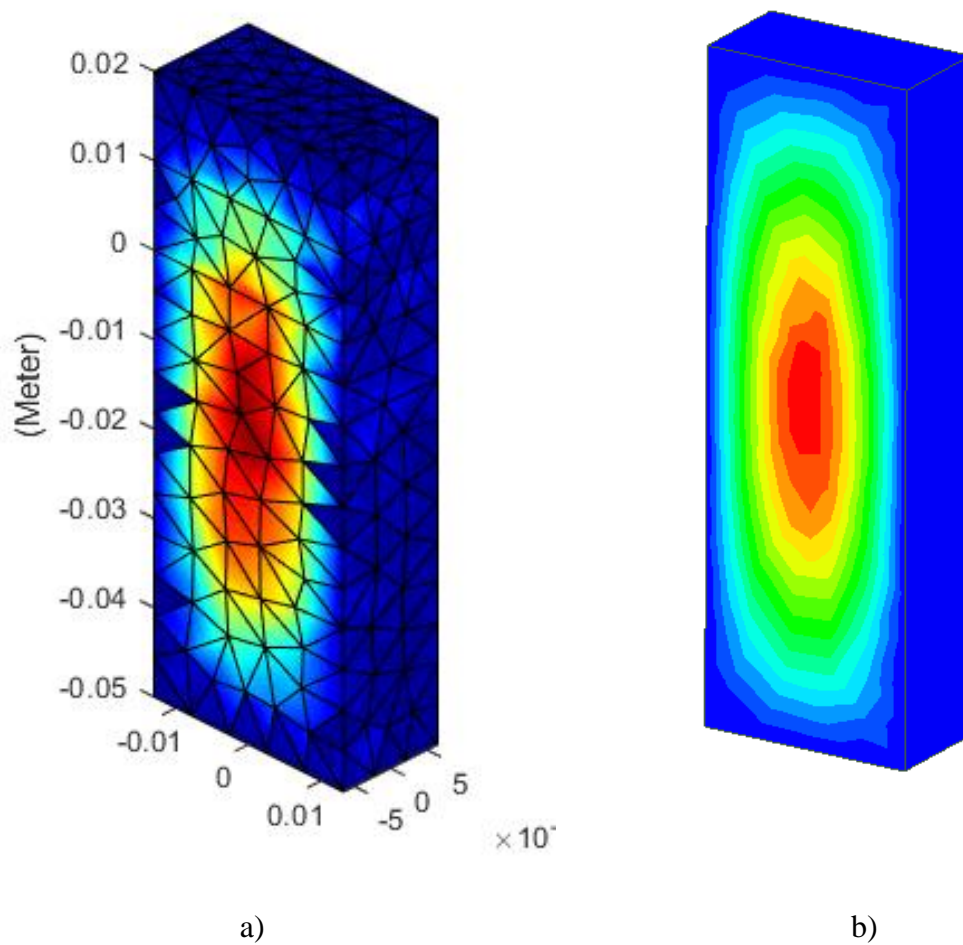


Figure 6: a) DG-FEM solution of the first eigenmode of dielectric cavity. b) HFSS solution of the same structure

As seen in Figure 6, the electric field distribution of the first mode is close to the solution obtained by the commercial program HFSS.

Table 4: Solution time and memory usage of Eigenmode solver

Solver	Solving time	Memory
DG-FEM	186s	75 MB
HFSS	3s	35 MB

The system used for obtaining the solution is equipped with an Intel i5-4200H CPU and 12GB RAM. Table 4 compares the solution times with the commercial code HFSS. It can be seen that the DG-FEM method is significantly slower. However, no special optimization has been conducted to accelerate the code. Since this study focuses solely on the validation and application of the method, there is ample room for improvement

In conclusion, the eigenvalue problem for the cavity was successfully solved using the Discontinuous Galerkin Finite Element Method (DG-FEM). The results, including the calculated and exact cutoff frequencies, show good agreement, thereby validating the accuracy and effectiveness of the numerical solver. The implementation of PEC boundary conditions was crucial in obtaining realistic results. In the next step, ports will be defined on the surfaces of the computational domain chosen to define the cavity to solve the waveguide structure.

3.2 Application of DG method to Waveguide Structures

In this chapter, the Discontinuous Galerkin Finite Element Method (DG-FEM) is applied to the analysis of waveguide structures. The same mesh used for the cavity, consisting of 1902 tetrahedral elements, is employed. However, two port surfaces are defined, and ABCs are implemented to simulate the waveguide's open boundaries. The introduction of ports and ABCs allows for the accurate simulation

of wave propagation and reflection within the waveguide. The implementation process will be given in this section, and results will be presented, including the electric field distributions and S-parameter calculations. The results are then compared with those obtained from the commercial software, HFSS, to validate the accuracy and effectiveness of the DG-FEM approach. Figure 7 shows the mesh structure and port surfaces.

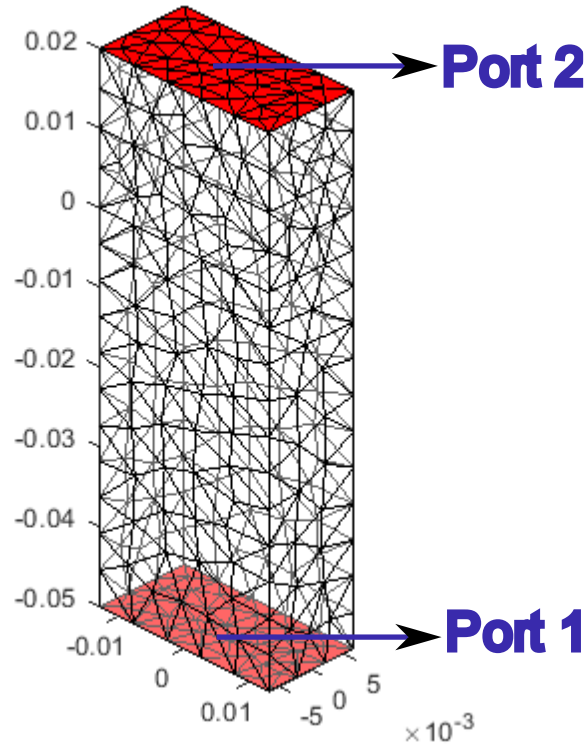


Figure 7: Waveguide structures and port surfaces

One of the most preferred methods for defining absorbing boundary conditions is the Silver-Müller radiation condition. The equation for this type of boundary condition is as follows [16]:

$$(\nabla \times \vec{E}) \times n - iw\sqrt{\epsilon}(n \times \vec{E}) \times n = (\nabla \times \vec{E}^i) \times n - iw\sqrt{\epsilon}(n \times \vec{E}^i) \times n \quad (3.3)$$

Here, E^i represents the incident field, which refers to the electric field defined at the port entrance. For the port surface, the TE₁₀ mode will be defined as the

incident mode. The commonly accepted method for determining the TE₁₀ mode involves solving the 2D eigenvalue problem on the port surface to identify the first mode. However, within the scope of this study, the analytical solution for the TE₁₀ mode has been utilized. This approach simplifies the implementation process while ensuring the accuracy of the boundary conditions. By using the analytical solution, it is possible to directly apply the TE₁₀ mode as the incident field, facilitating the simulation of wave propagation within the waveguide structure. The analytically calculated port field is shown in Figure 8.

$$E_x = A_{mn} \frac{\beta_y}{\epsilon} \cos(\beta_x x) \sin(\beta_y y) e^{-j\beta_z z} \quad (3.4)$$

$$E_y = -A_{mn} \frac{\beta_x}{\epsilon} \sin(\beta_x x) \cos(\beta_y y) e^{-j\beta_z z} \quad (3.5)$$

$$E_z = 0 \quad (3.6)$$

$$H_x = A_{mn} \frac{\beta_x \beta_z}{\omega \mu \epsilon} \sin(\beta_x x) \cos(\beta_y y) e^{-j\beta_z z} \quad (3.7)$$

$$H_y = A_{mn} \frac{\beta_y \beta_z}{\omega \mu \epsilon} \cos(\beta_x x) \sin(\beta_y y) e^{-j\beta_z z} \quad (3.8)$$

$$H_z = A_{mn} \frac{\beta_x^2 + \beta_y^2}{\omega \mu \epsilon} \cos(\beta_x x) \cos(\beta_y y) e^{-j\beta_z z} \quad (3.9)$$

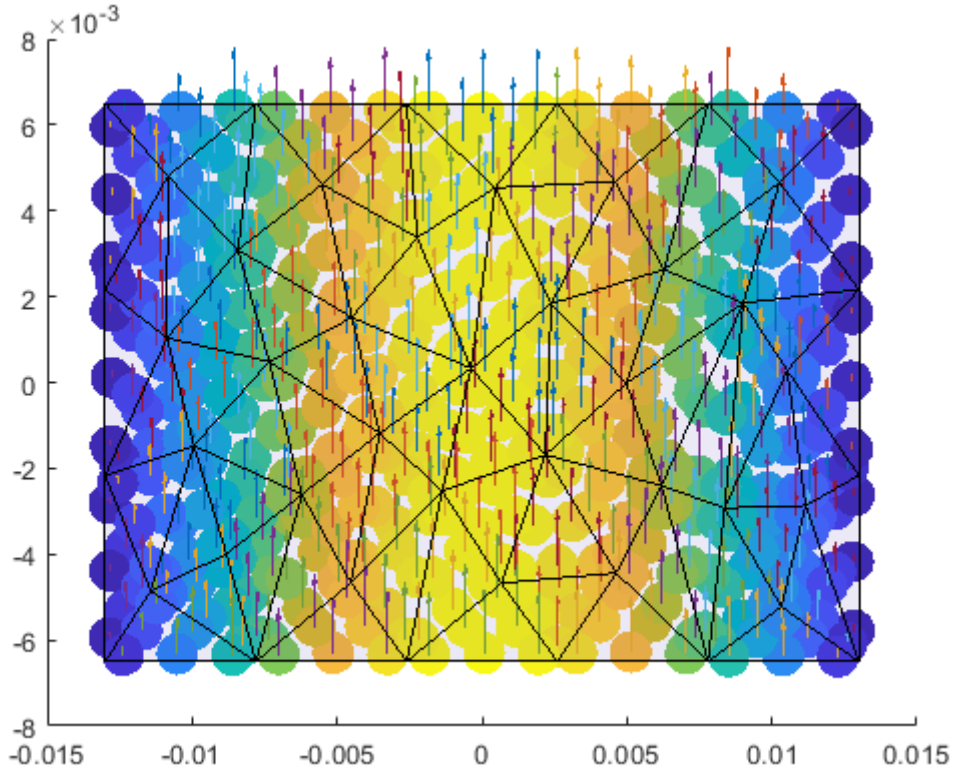


Figure 8: Analytically calculated TE10 mode on the port surface

By testing Equation ((3.3), we obtain the following equation:

$$\begin{aligned}
 & \int \left((\nabla \times \vec{E}) \times n \right) \cdot \phi \, dx - iw\sqrt{\varepsilon} \int \left((n \times \vec{E}) \times n \right) \cdot \phi \, dx \\
 & = \int \left((\nabla \times \vec{E}^i) \times n \right) \cdot \phi \, dx 1 - iw\sqrt{\varepsilon} \int \left((n \times \vec{E}^i) \times n \right) \cdot \phi \, dx
 \end{aligned} \tag{3.10}$$

The basis functions can be written as:

$$\vec{E} = \sum_{j=1}^{np} u_{j,K} \psi_{j,K} \tag{3.11}$$

$$\nabla \times \vec{E} = \sum_{j=1}^{np} u_{j,K} \nabla \times \psi_{j,K} \tag{3.12}$$

Applying equation ((3.11) and ((3.12) to equation ((3.10) yields:

$$\begin{aligned}
& \sum_{j=1}^{np} u_{j,K} \int \left((\nabla \times \psi_{j,K}) \times n \right) \cdot \phi \, dx - iw\sqrt{\varepsilon} \sum_{j=1}^{np} u_{j,K} \int \left((n \times \psi_{j,K}) \times n \right) \cdot \phi \, dx \\
& = \int \left((\nabla \times E^i) \times n \right) \cdot \phi \, dx - iw\sqrt{\varepsilon} \int \left((n \times E^i) \times n \right) \cdot \phi \, dx
\end{aligned} \tag{3.13}$$

Equation (3.13) includes the implementation of the absorbing boundary condition at the ports. The remaining surfaces should be defined as PEC (Perfect Electric Conductor). This configuration effectively models the waveguide structure. Once the necessary adjustments are made for this setup, the electric field distribution within the waveguide at a single frequency can be calculated using the DG-FEM method. The projection of the calculated field on the port surface onto the incident electric field will provide the reflection parameters. This method ensures that the waveguide's behavior is accurately captured, allowing for detailed analysis of the electromagnetic wave interactions within the structure.

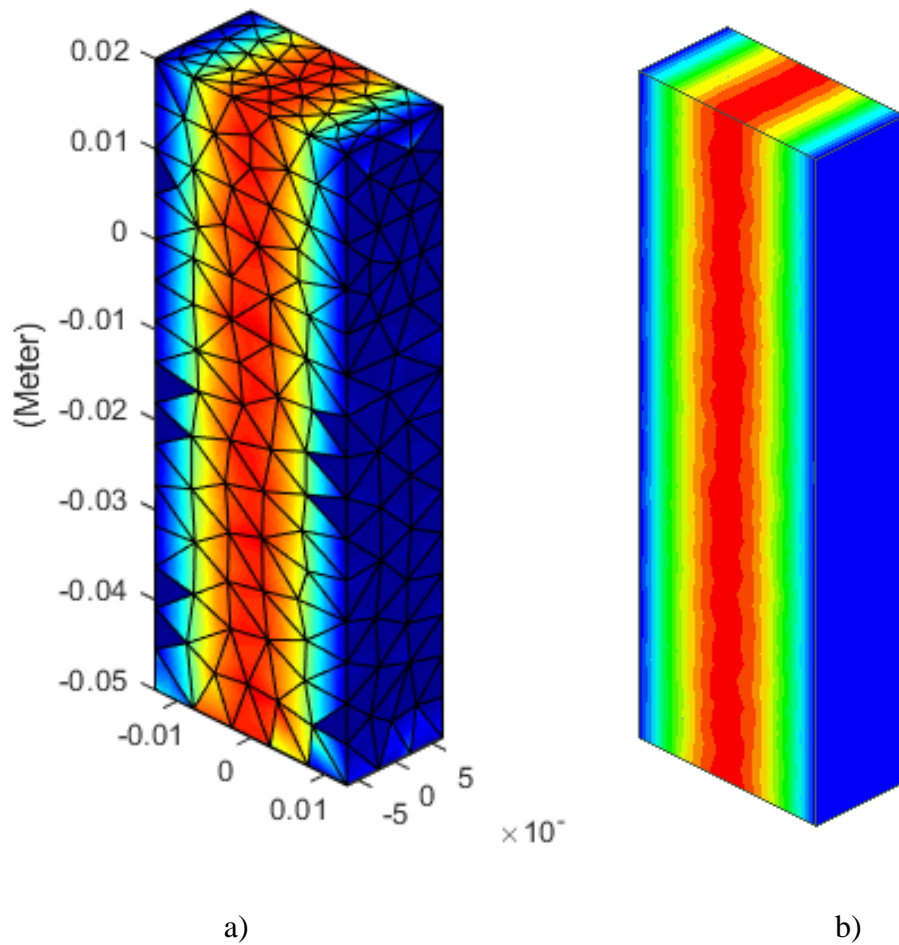


Figure 9: a) DG-FEM solution of complex magnitude of waveguide E field. b) HFSS solution of the same structure

Figure 9 shows the flow of electric field energy within the waveguide from one port to the other. The absence of reflections in this field distribution indicates that the port models and the simulation are functioning correctly. However, for a comprehensive comparison, solutions should be obtained at intervals of 250 MHz between 5 GHz and 10 GHz, and the S11 parameter should be calculated for each frequency. The calculated S11 parameter will be compared with the solutions obtained from HFSS and OpenEMS.

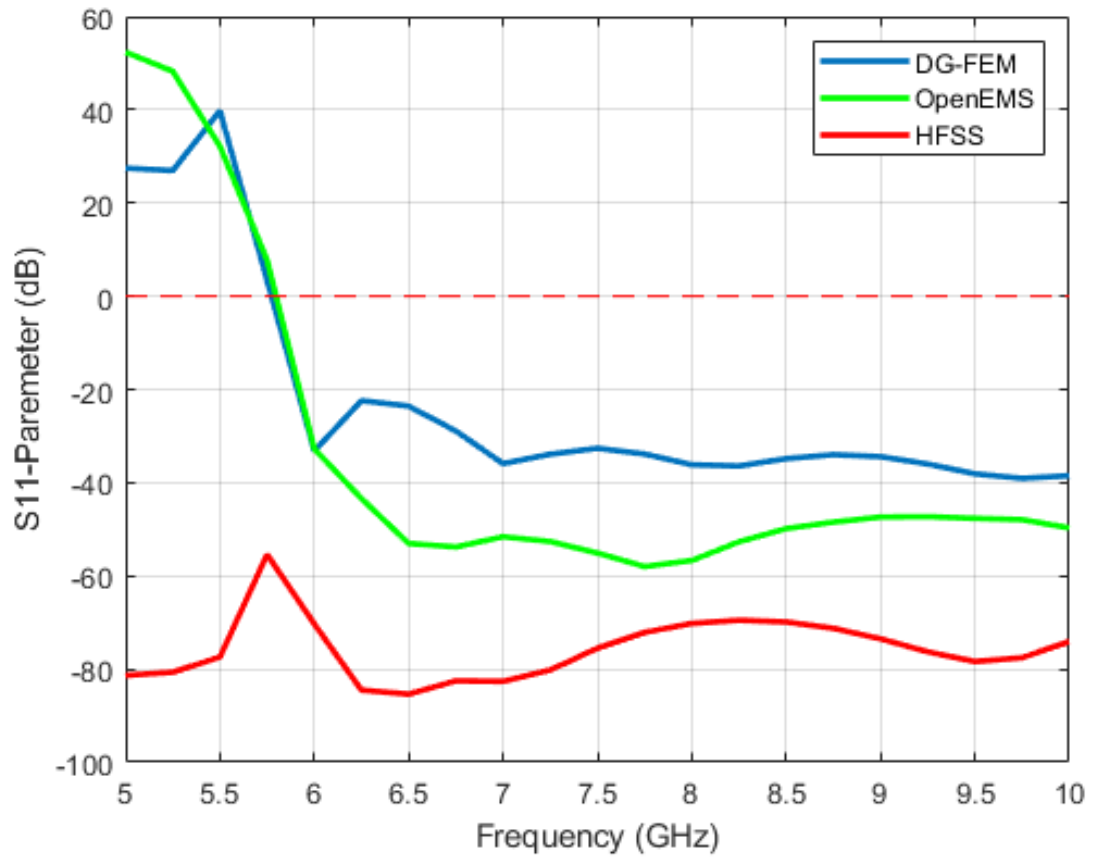


Figure 10: The comparison of S11 parameter of the waveguide structure with results from different solvers

Figure 10 compares the results obtained using the DG-FEM method presented in this study with those from other commercial solvers. The results below 6 GHz are spurious solutions as they are below the cutoff frequency.

Table 5: Solution time and memory usage of Waveguide solver

Solver	Solution time	Memory
DG-FEM	216s	75 MB
HFSS	9s	43 MB

Table 5 shows the simulation times. It can be said that the solution times have increased slightly in the waveguide structure, although the same mesh structure used for the cavity problem is employed. However, the lack of time optimization in the DG-FEM method maintains the time and memory size differences between the methods.

3.3 Simulation and Analysis of Microstrip Structures Using DG Method

In this section, the Discontinuous Galerkin Finite Element Method (DG-FEM) is applied to the analysis of a microstrip structure. In this section, the simulation setup includes a substrate with dimensions of 100x100mm and a thickness of 3mm. The material used for the substrate is FR4, which has a relative dielectric constant of 4.4. On top of the substrate, a microstrip line with a width of 4mm is implemented. Figure 11 shows the structure and the mesh grid. A ground layer is located beneath the substrate. Both the ground and the microstrip line are modeled as PEC. Two ports are placed at the beginning and end of the line. The ports are defined using the ABC as described for the waveguide structure, and the port fields are analytically calculated. The port field is shown in Figure 12. The entire setup is enclosed in a vacuum cube with a side length of 150mm. The surfaces of the cube are surrounded by a 60mm thick layer of Perfectly Matched Layer (PML) material [17]-[18]. The results are then compared with those obtained from the commercial software HFSS, to validate the accuracy and effectiveness of the DG-FEM approach. The following figures illustrate the comparison of field distributions and S-parameters for the microstrip line.

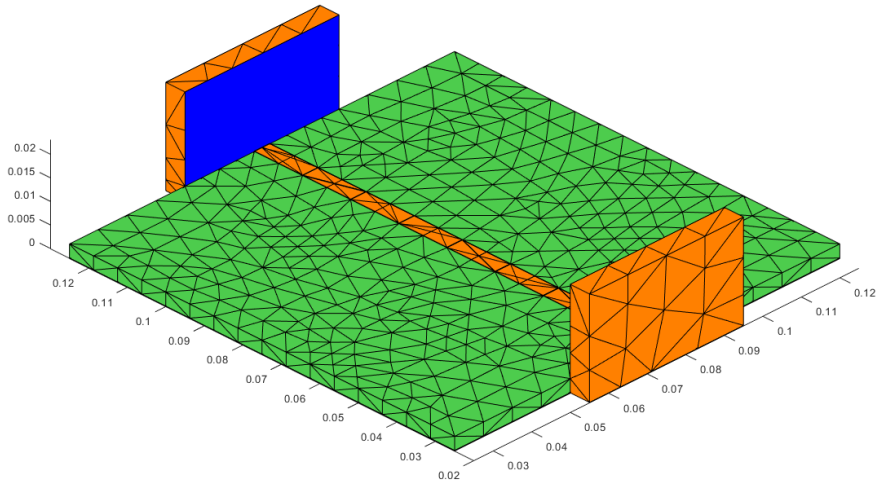


Figure 11: Mesh structure and port surfaces of the microstrip line

The mesh structure and port surfaces of the microstrip line are shown. The analytical solution for the port field is utilized to accurately define the incident field. The mesh consists of 21263 tetrahedral elements, ensuring detailed modeling of the microstrip structure.

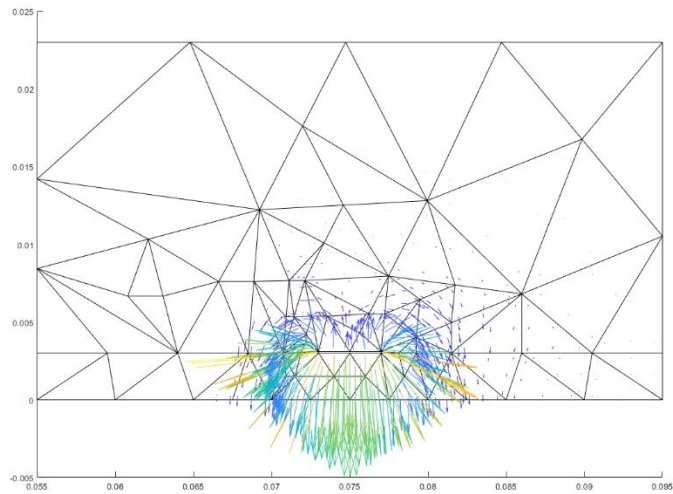


Figure 12: Electric field distribution on the port surface of the microstrip line

The electric field distribution on the port surface is depicted in Figure 12. The analytically calculated port field shows the expected field distribution, providing a reliable basis for the simulation.

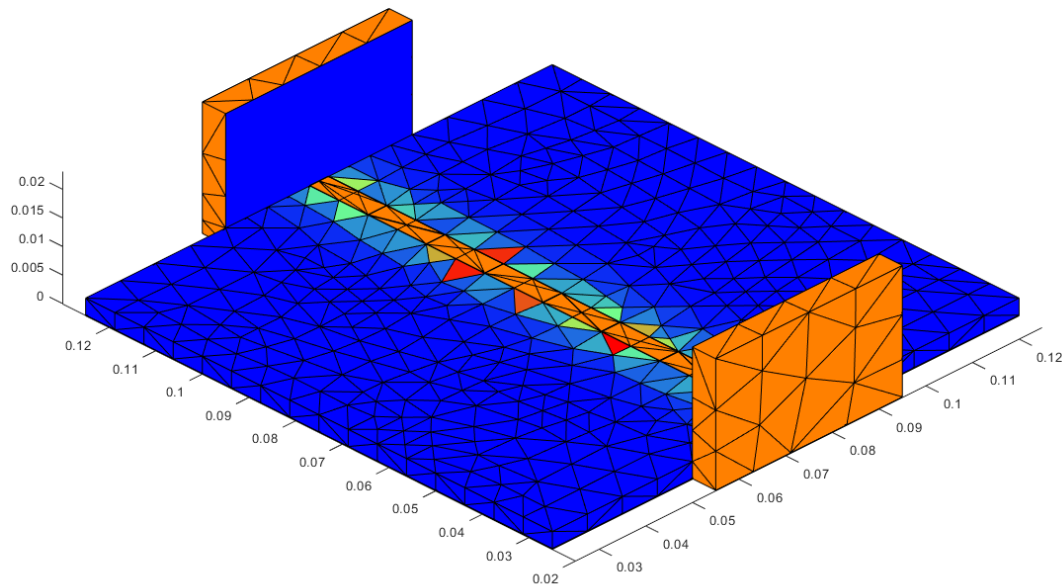


Figure 13: Electric field distribution along the microstrip line

The electric field distribution along the microstrip line solution at 10 GHz is shown in Figure 13. The DG-FEM solution demonstrates accurate modeling of the field propagation along the microstrip line, with the absence of reflections indicating correct functioning of the ports and simulation.

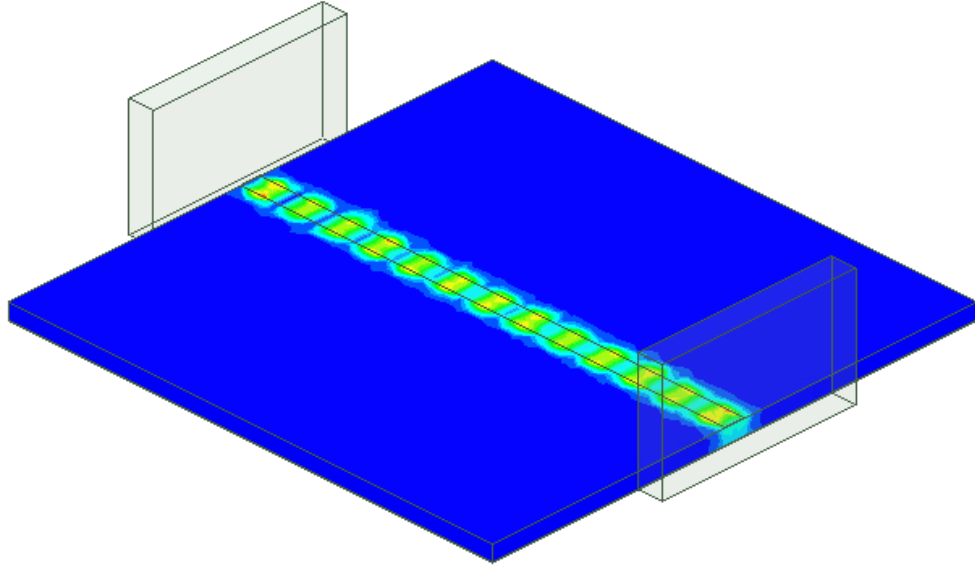


Figure 14: HFSS solution of the electric field distribution along the microstrip line

The HFSS solution of the electric field distribution along the microstrip line is presented in Figure 14. When comparing the results of the DG-FEM method with the HFSS solution in terms of the field distribution, the DG-FEM results may appear different due to the field being plotted as a single color over the mesh and the low mesh resolution. It can be stated that the field distributions are similar and that power transmission is achieved.

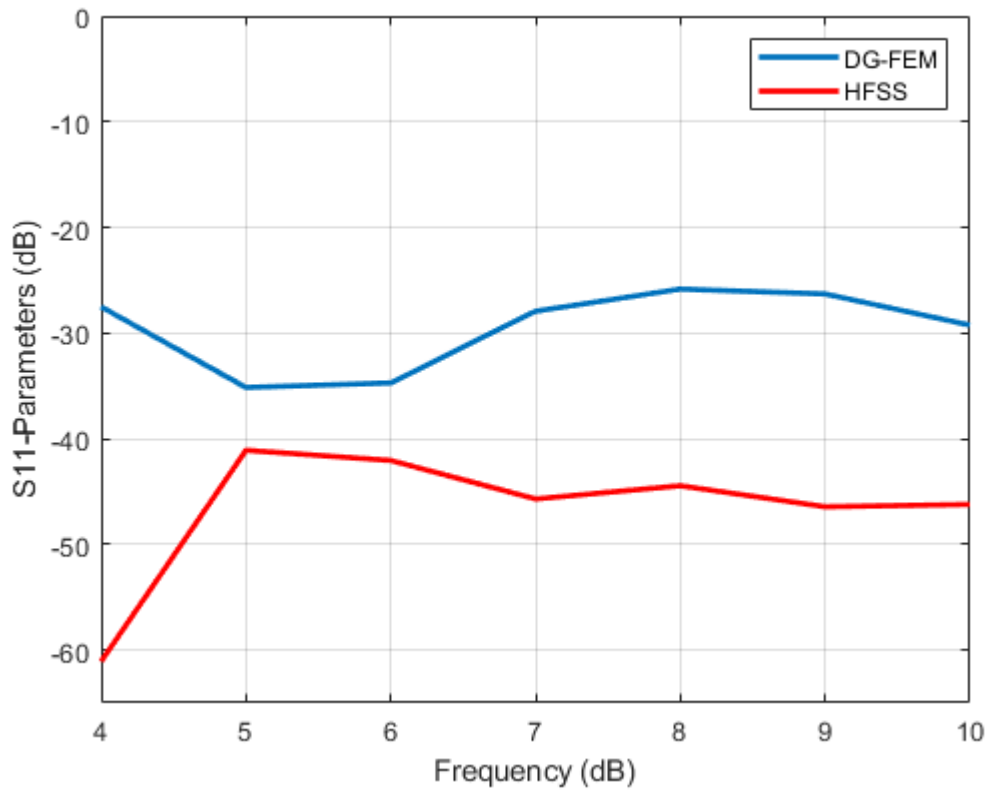


Figure 15: S11-parameters of the microstrip line

Figure 15 illustrates the S11-parameter which is the reflection coefficient of the microstrip line. The results are compared with those obtained from HFSS. It is also observed that the DG-FEM method does not go below -35 dB. The calculated S11 parameter provides insight into the reflection characteristics of the microstrip line. It can be concluded that the reflection is low and transmission is achieved.

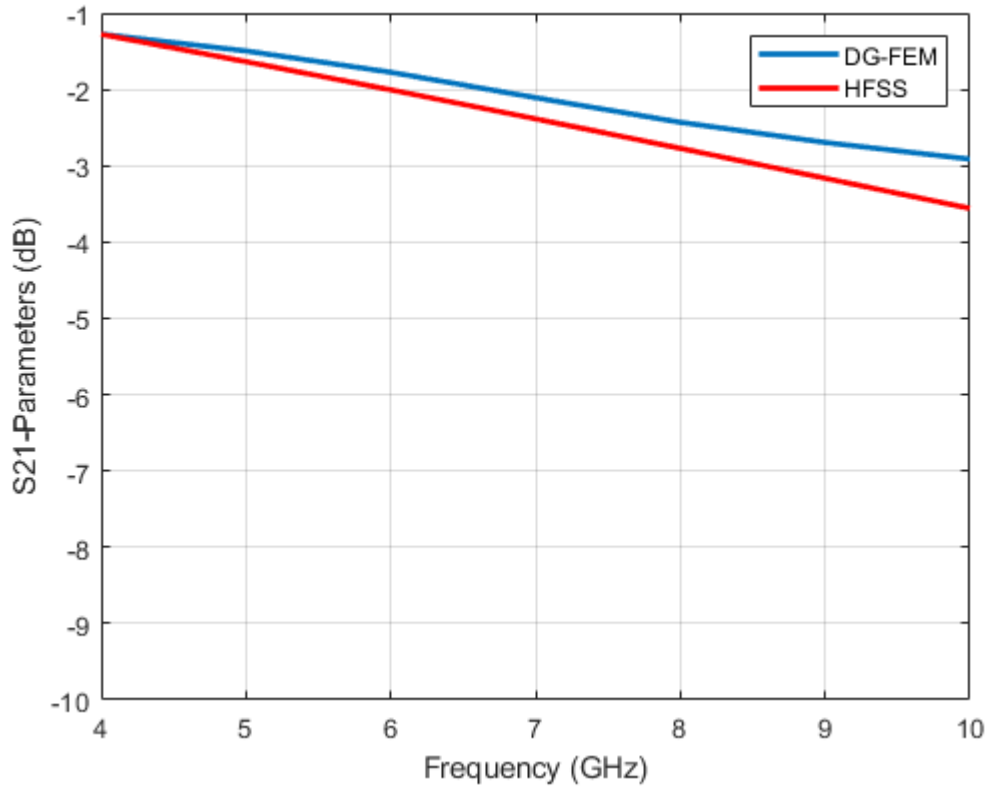


Figure 16: Comparison of S-parameters from different solvers

Figure 16 compares the S21-parameters obtained from the DG-FEM method, and HFSS solution. The consistency of the results across different solvers demonstrates the reliability and effectiveness of the DG-FEM approach for microstrip structure analysis.

By implementing PML at the boundaries and accurately defining the port fields, the DG-FEM method provides precise simulation of microstrip structures. The results, including field distributions and S-parameters, show agreement with those from commercial solvers, validating the approach's accuracy. This comprehensive analysis highlights the potential of DG-FEM for detailed electromagnetic simulation of microstrip structures.

Table 6: Solution time and memory usage of Microstrip solver

Solver	Solution time	Memory
DG-FEM	83m	2.65 GB
HFSS	2m 40s	1.15 GB

Table 6 shows the solution times and memory values for the microstrip problem. The asymmetry in solution times is also evident here. To solve the line at a high frequency, such as 10 GHz, the number of elements had to be increased. This explains the increase in solution times and memory requirements.

3.4 Antenna Structure

In this section, the DG-FEM method is applied to the simulation and analysis of an antenna structure, with a computational domain similar to the previous microstrip structure. The simulation setup includes a substrate with dimensions of 60x60mm and a dielectric constant of 4.4, made of FR4 material. The patch antenna on the substrate has dimensions of 32x40mm, with the microstrip line positioned 5.5mm away from the center.

The antenna is enclosed in a vacuum cube with an edge length of 100mm, surrounded by a 40mm thick PML material on the cube surfaces to simulate open boundaries. By employing the same port setup and analytical port field as in the microstrip simulation, the accuracy and consistency of the DG-FEM method are validated.

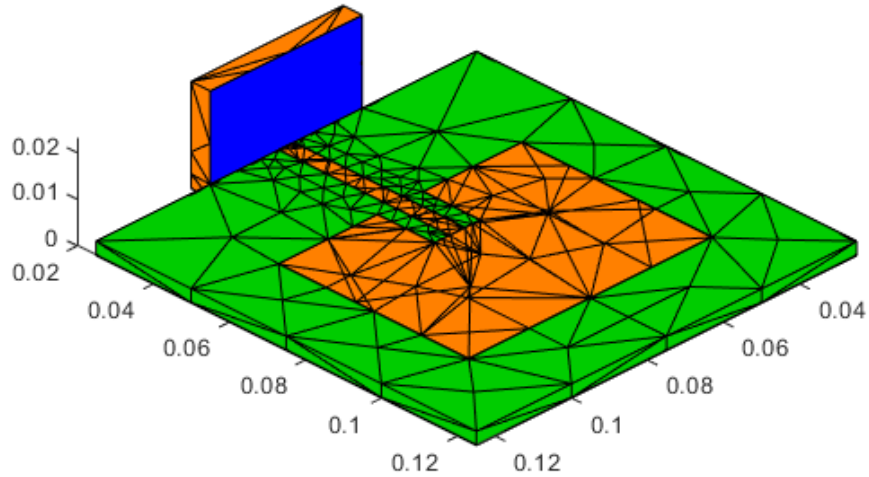


Figure 17: Mesh structure of the antenna

In Figure 17, the detailed setup of the substrate, patch, and microstrip line is highlighted. The mesh structure consists of 7863 tetrahedral elements. The port field used for this antenna simulation is identical to the port field used in the microstrip simulation. The S_{11} parameter graph for the antenna is presented in Figure 18, illustrating the performance of the antenna and providing a comparison between the simulated and expected results.

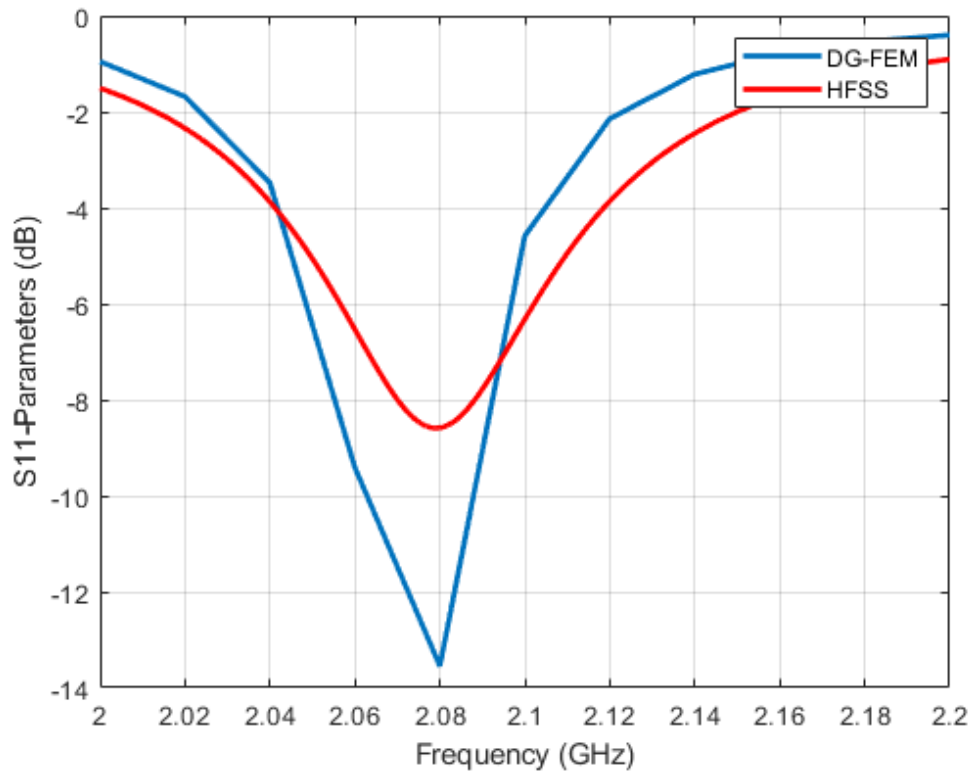


Figure 18: S11 parameter graph for the antenna structure

Figure 18 shows the reflection coefficient of the antenna structure between 2 GHz and 2.2 GHz. The results indicate that at a frequency of 2.08 GHz, the structure is capable of coupling energy to the surroundings, as radiated field. While this demonstrates the effectiveness of the DG-FEM method, it can be noted that the difference in S11 parameters can vary by up to 5dB, indicating a relatively high error margin.

Table 7: Solution time and memory usage of antenna solver

Solver	Solution time	Memory
DG-FEM	344s	97 MB
HFSS	5s	53 MB

Table 7 shows the solution times and memory usage for the antenna problem. The solution time of the DG-FEM method is longer and uses more memory compared to the HFSS solver. The fact that the memory required for all four solutions is twice as much as that used in HFSS is consistent with the DG-FEM method using discontinuous bases, which effectively doubles the number of unknowns.

CHAPTER 4

CONCLUSION

In this thesis, the Discontinuous Galerkin Finite Element Method (DG-FEM), has been thoroughly presented through some applications, and its place among various numerical methods such as Finite Difference Time Domain (FDTD), Method of Moments (MoM), and Finite Element Method (FEM) has been discussed. The analysis starts with Maxwell's equations, and the vector wave equation has been derived from these equations. In order to solve this equation, the equation is converted to a form suitable for the DG method, in other words it has been transformed to the weak formulation. The interior penalty term has been introduced, leading to the formulation of the general final form of the equation. Nedelec basis functions, which are crucial for the implementation of DG-FEM, have been introduced and explained. The stiffness, mass, and flux matrices have been derived, forming the core components of the method.

Practical results have been obtained to validate the method. The algorithm has been introduced, followed by the definition of the eigenvalue problem for a cavity. A cavity model has been presented, characterized by a computational domain with dimensions of 70x26x13 mm and comprising 1902 tetrahedral elements, with boundary walls defined as PEC. The PEC boundary condition has been introduced, and it has been shown that the cavity modes were correctly calculated, with accurate identification of cutoff frequencies. The field for the first mode was plotted and compared with the HFSS solution, confirming the correctness of the DG-FEM solution. Although the solution time for this structure was 186 seconds compared to 3 seconds for HFSS, it was emphasized that time optimization was not the objective, as the focus was on method validation.

Next, a waveguide structure has been introduced. The computational domain was similar to that of the cavity, with the addition of two ports defined by ABC. An overview of ABC was provided, and the incident field for the ports was calculated analytically. It was suggested that in future work, an eigenvalue problem could be solved on the port surface to identify modes, with the first mode used as the incident field. Transmission was observed in the waveguide structure, and S parameters were obtained. These parameters were found to be consistent with HFSS results, although the DG-FEM implementation failed to achieve a reflection value below -35 dB due to noise. This issue was identified as an area for future improvement. The solution times remained long, and memory usage was twice that of HFSS, attributed to the use of discontinuous bases in DG-FEM, effectively doubling the number of unknowns. Nevertheless, the waveguide structure was considered the most valuable validation of the method, as it required simultaneous implementation of ABC port and PEC boundary conditions.

The microstrip structure has been the next problem to be discussed. This problem involved PML, PEC, and ABC at the ports, similar to the waveguide structure, but adapted to the microstrip geometry. The microstrip structure was solved in the frequency range of 4-10 GHz, resulting in a large number of elements. The results were similar to those of the waveguide, with the S11 parameter failing to drop below -35 dB, while the S21 parameter closely matched HFSS results, with a maximum difference of 0.6 dB. It was noted that future work should aim to reduce this discrepancy and investigate the factors contributing to the error. The solution times indicated that the current implementation of the DG-FEM method was not suitable for design purposes, highlighting the need for optimization in future studies.

Finally, an antenna structure was analyzed. The S11 parameters demonstrated that resonance is achieved at the same frequency as the HFSS solution, but with an error of around 5 dB. This error, as previously mentioned, could be attributed to noise in the solver and should be addressed in future work.

Overall, the DG-FEM method offers significant potential for new research due to the ease of connecting different domains through boundary conditions. Different domains can be linked solely through boundary condition definitions, making the DG-FEM method a promising tool for future studies. The work presented in this thesis demonstrates the method's validity and application, but also highlights areas for improvement, particularly in terms of solution time and accuracy. Further research and development are required to enhance the performance of the DG-FEM method, ensuring its suitability for practical engineering applications.

REFERENCES

- [1] D. M. Pozar, Microwave Engineering, 4th Edition. Wiley, 2011.
- [2] C. Balanis, “Advanced Engineering Electromagnetics,” John Wiley & Sons, Hoboken, 1989.
- [3] J. L. Volakis, A. Chatterjee, and L. C. Kempel, Finite Element Method Electromagnetics: Antennas, Microwave Circuits, and Scattering Applications. Wiley, 1998.
- [4] D. L. Darmofal, “An Introduction to Discontinuous Galerkin Methods for Compressible Flows,” MIT, [https:// https://acdl.mit.edu/IntroToDG.pdf](https://acdl.mit.edu/IntroToDG.pdf) (accessed July 31, 2024).
- [5] J. M. Jin, The Finite Element Method in Electromagnetics, 3rd ed. Wiley, 2015.
- [6] P. Monk, Finite Element Methods for Maxwell’s Equations. Oxford University Press, 04 2003.
- [7] C. Shu, “Discontinuous galerkin methods: general approach and stability. Numerical solutions of partial differential equations,” Brown University, 2009
- [8] B. Cockburn. “Discontinuous Galerkin methods. Journal of Applied Mathematics and Mechanics” Zeitschrift für Angewandte Mathematik und Mechanik, 2003, 83 (11), pp.731-754.
- [9] L. Chen, “Finite Element Methods For Maxwell Equations,” math.uci.edu, <https://www.math.uci.edu/~chenlong/226/FEMMaxwell.pdf> (accessed July 31, 2024).

- [10] D. Doğan “Fast And Accurate Analysis Of Phased Array Antennas Using A Hybrid Discontinuous Galerkin Finite Element Domain Decomposition Scheme ” Middle East Technical University, 2023
- [11] I. Denissen, “Discontinuous Galerkin Finite Element Methods for the time-harmonic Maxwell equations in periodic media,” University of Twente, 2013.
- [12] J. C. Nédélec, “Mixed finite elements in R^3 ,” *Num. Math.*, vol. 35, pp. 315-341, 1980.
- [13] P. Solin, K. Segeth, and I. Dolezel, *Higher-Order Finite Element Methods*. CRC Press, 2003.
- [14] D. N. Arnold, F. Brezzi, B. Cockburn, and L. D. Marini, “Unified analysis of discontinuous Galerkin methods for elliptic problems,” *SIAM J. Numer. Anal.*, vol. 39, no. 5, pp. 1749–1779, 2002.
- [15] J. Scott Savage and A. F. Peterson, “Higher-Order Vector Finite Elements for Tetrahedral Cells,” *IEEE Trans. Microw. Theory Tech.*, vol. 44, no. 6, pp. 874–879, 1996.
- [16] P. Monk, “Finite Element Methods for Maxwell’s Equations,” *Icerm*, https://icerm.brown.edu/materials/Slides/tw-18-7/Finite_Element_Methods_for_Maxwells_Equations_%5D_Peter_Monk,_University_of_Delaware.pdf (accessed July 31, 2024).
- [17] J.-P. Berenger, “A perfectly matched layer for the absorption of electromagnetic waves,” *J. Comput. Phys.*, vol. 114, no. 2, pp. 185–200, 1994.
- [18] M. Kuzuoglu and R. Mittra, "Frequency dependence of the constitutive parameters of causal perfectly matched anisotropic absorbers," in *IEEE Microwave and Guided Wave Letters*, vol. 6, no. 12, pp. 447-449, Dec. 1996, doi: 10.1109/75.544545.